NAVAL POSTGRADUATE SCHOOL

MONTEREY, CALIFORNIA

THESIS

VERIFICATION OF AEROSOL OPTICAL DEPTH RETRIEVALS FROM CLOUD SHADOWS USING SATELLITE IMAGERY

by

Perry Courtney Sweat

March 2008

Thesis Advisor:	Philip A. Durkee
Second Reader:	Kurt Nielsen

Approved for public release; distribution is unlimited.

THIS PAGE INTENTIONALLY LEFT BLANK

REPORT DOCUMENTATION PAGE			Form Approved OMB No. 0704-0188
Public reporting burden for this collection of information is estimated to average 1 hour per response, including the time for reviewing instruction, searching existing data sources, gathering and maintaining the data needed, and completing and reviewing the collection of information. Send comments regarding this burden estimate or any other aspect of this collection of information, including suggestions for reducing this burden, to Washington headquarters Services, Directorate for Information Operations and Reports, 1215 Jefferson Davis Highway, Suite 1204, Arlington, VA 22202-4302, and to the Office of Management and Budget, Paperwork Reduction Project (0704-0188) Washington DC 20503.			
1. AGENCY USE ONLY *(Leave blank)*	**2. REPORT DATE** March 2008	**3. REPORT TYPE AND DATES COVERED** Master's Thesis	
4. TITLE AND SUBTITLE Verification of Aerosol Optical Depth Retrievals using Cloud Shadows Retrieved from Satellite Imagery		**5. FUNDING NUMBERS**	
6. AUTHOR(S) Perry C. Sweat			
7. PERFORMING ORGANIZATION NAME(S) AND ADDRESS(ES) Naval Postgraduate School Monterey, CA 93943-5000		**8. PERFORMING ORGANIZATION REPORT NUMBER**	
9. SPONSORING /MONITORING AGENCY NAME(S) AND ADDRESS(ES) N/A		**10. SPONSORING/MONITORING AGENCY REPORT NUMBER**	
11. SUPPLEMENTARY NOTES The views expressed in this thesis are those of the author and do not reflect the official policy or position of the Department of Defense or the U.S. Government.			
12a. DISTRIBUTION / AVAILABILITY STATEMENT Approved for public release; distribution is unlimited.		**12b. DISTRIBUTION CODE**	

13. ABSTRACT (maximum 200 words)

A technique for deriving aerosol optical depths by measuring the radiance inside and outside of shaded regions is expanded to include shadows from clouds. Previous research focused on utilizing QuickBird satellite imagery. The 2.4 meter resolution of QuickBird allowed for sampling to focus on building-generated shadows. Research was done on several different surface types, including dirt, grass, sand, and pavement. The research presented in this thesis focuses on the challenges presented by attempting this technique with three other types of imagery—Moderate Resolution Imaging Spectrometer (MODIS), IKONOS, and Advanced Spaceborne Thermal Emission and Reflection Radiometer (ASTER). The lower resolution of MODIS and ASTER does not lend itself to focusing on building shadows, but rather cloud shadows. Results from sampling cloud-generated shadows show this method has promise, much like previous studies and opens up aerosol optical depth determination using this technique to a wide variety of imagery as well as additional sensor platforms.

14. SUBJECT TERMS Aerosol, Shadow Method, QuickBird, ASTER, MODIS, IKONOS, Aerosol Optical Depth Retrieval, Cloud Shadows			**15. NUMBER OF PAGES** 86
			16. PRICE CODE
17. SECURITY CLASSIFICATION OF REPORT Unclassified	**18. SECURITY CLASSIFICATION OF THIS PAGE** Unclassified	**19. SECURITY CLASSIFICATION OF ABSTRACT** Unclassified	**20. LIMITATION OF ABSTRACT** UU

NSN 7540-01-280-5500 Standard Form 298 (Rev. 2-89)
Prescribed by ANSI Std. 239-18

THIS PAGE INTENTIONALLY LEFT BLANK

Approved for public release; distribution is unlimited.

VERIFICATION OF AEROSOL OPTICAL DEPTH RETRIEVALS FROM CLOUD SHADOWS USING SATELLITE IMAGERY

Perry C. Sweat
Captain, United States Air Force
B.S., Florida State University, 2003

Submitted in partial fulfillment of the
requirements for the degree of

MASTER OF SCIENCE IN METEOROLOGY

from the

NAVAL POSTGRADUATE SCHOOL
March 2008

Author: Perry C. Sweat

Approved by: Philip A. Durkee
Thesis Advisor

Kurt E. Nielsen
Second Reader

Philip A. Durkee
Chairman, Department of Meteorology

THIS PAGE INTENTIONALLY LEFT BLANK

ABSTRACT

A technique for deriving aerosol optical depths by measuring the radiance inside and outside of shaded regions is expanded to include shadows from clouds. Previous research focused on utilizing QuickBird satellite imagery. The 2.4 meter resolution of QuickBird allowed for sampling to focus on building-generated shadows. Research was done on several different surface types, including dirt, grass, sand, and pavement. The research presented in this thesis focuses on the challenges presented by attempting this technique with three other types of imagery—Moderate Resolution Imaging Spectrometer (MODIS), IKONOS, and Advanced Spaceborne Thermal Emission and Reflection Radiometer (ASTER). The lower resolution of MODIS and ASTER does not lend itself to focusing on building shadows, but rather cloud shadows. Results from sampling cloud-generated shadows show this method has promise, much like previous studies, and opens up aerosol optical depth determination using this technique to a wide variety of imagery as well as additional sensor platforms.

THIS PAGE INTENTIONALLY LEFT BLANK

TABLE OF CONTENTS

LIST OF FIGURES

LIST OF TABLES

ACKNOWLEDGMENTS

I would like to thank Professor Philip Durkee and Kurt Nielsen for their assistance and dedication to a topic of which I had limited knowledge from the beginning. Their willingness to answer questions at a moment's notice, particularly when this was first discussed as a possible research topic, was key to understanding the fundamentals and ultimately the results.

Second, I would like to thank my wife Rebecca for her patience and understanding into the effort required to complete this nearly two year journey. Her unwavering support was key to accomplishing this goal in my life and for that I am grateful.

THIS PAGE INTENTIONALLY LEFT BLANK

I. INTRODUCTION

Aerosol particles are tiny particles of matter suspended in the atmosphere that range in size from less than ten nanometers to more than 100 micrometers. Aerosol particles are classified as either natural or anthropogenic. Natural sources of aerosol particles include forest fires, wind-blown dust, volcanoes, and sea spray. Anthropogenic sources such as hydrocarbon combustion byproducts account for approximately ten percent of the aerosol particles in the atmosphere. As more research is done on the Earth's environment related to the global energy budget the effect of aerosol particles is being studied, particularly from anthropogenic sources. Aerosol particles scatter and absorb direct solar radiation. The amount of scattering and absorption varies according to aerosol properties. Aerosol particles can impact clouds by what is known as the Twomey Effect. Twomey (1974) observed that increasing aerosol concentrations in the atmosphere result in greater cloud condensation nuclei concentrations (CCN) resulting in increased cloud reflectance and reduced heating of the Earth's surface and atmosphere.

Atmospheric aerosol particles are of concern to military operations because these particles affect the way radiation is transmitted through the atmosphere. An increase in atmospheric aerosol particles can result in reduced visibility either horizontally on the battlefield or vertically from the air. Military air operations are becoming increasingly reliant on electro-optical data to determine the most efficient tactic to use. Having the ability to correctly characterize the atmosphere can be critical in selecting the correct weapon to use in a surgical strike. An accurate characterization of the atmosphere is vital to reconnaissance operations from air and space. Under adverse conditions, these operations can be severely degraded. From a physical meteorology standpoint, an increase in CCN could result in an unforeseen increase in clouds and precipitation or fog and could delay or cancel critical strike missions.

Quantifying aerosol properties on the battlefield in real time has proven difficult. Observation networks are generally not in place in hostile areas. Having the ability to determine optical depths anywhere in the world within a relatively short time span by means of satellite-based remote sensing has been the focus of much research over the past

few decades. While there has been significant and important advancement in remote sensing techniques and imagery, there are still limitations to retrieving optical depth and visibility information remotely. Remotely retrieving atmospheric optical properties is particularly problematic over brighter land surfaces.

The advancements and availability of high-resolution satellite imagery (e.g., imagery with five meter resolution or better) has encouraged and enabled new ideas to tackling the atmospheric optical properties problem. With new advancements in imagery, surface details never seen before are now available for exploitation. Vincent (2006) developed a technique known as the Shadow Method in which shadows of individual structures are identified and radiance samples are measured inside and outside of shadow. Atmospheric aerosol properties were then determined. Evans (2007) expanded on Vincent's work to include more detailed results of this technique in an urban environment and over different surface types. Both Vincent and Evans found this technique to have the potential to accurately retrieve optical depths over land. This thesis will study this method further and will apply it to much larger shadows generated by clouds using lower resolution meteorological satellite imagery. Just as building shadows were sampled in previous studies, cloud shadows can be sampled in much the same way. Clouds of suitable vertical and horizontal extent generate shadows that can be effectively sampled to determine the direct radiance transmission, and the optical depth of the atmosphere can be calculated. Successfully applying this technique to cloud shadows will open it up to not just cloud-free high-resolution imagery where surface structures are casting shadows but also to any imagery with shadow generators. This thesis will also study this technique using satellite sensors of differing spatial resolutions to determine its limitations.

II. BACKGROUND

A. RELATED RESEARCH

1. Contrast Reduction Method

The earliest attempts to determine aerosol effects began with what is known as the Contrast Reduction Method. This technique by Odell and Weinman (1975) took two surface objects with differing albedo and compared the radiance values from both. A relationship could then be established between the aerosol optical depth and the measured radiances. This relationship hinged on a contrast transmission function that is based on aerosol optical depth, mean surface reflectance, and sun-sensor geometry. Later research by Kaufman and Joseph (1982) focused on imagery with discontinuities in albedo, such as along a coastline. The image could be divided into two-halves with different albedo values, and then aerosol characteristics could be retrieved through automated procedures. Sensitivity studies showed that this procedure was highly sensitive to single scattering albedo and optical depth.

2. Dark Object Method

One of the oldest and most basic methods for determining aerosol characteristics is known as the Dark Object Method. This method proved useful over regions of dense dark vegetation where surface reflectance is negligible. Kaufman and Sendra (1988) developed an algorithm to automate atmospheric corrections using this method. An assumed surface reflectance was used for dark regions and any radiance measured beyond that was attributed to scattering from aerosol particles. The algorithm is sensitive to the *assumed* reflectance of the dark vegetation. Another disadvantage to this method is that it can not be applied everywhere. It is only effective in regions of dark dense vegetation where the characteristics of the vegetation are known. However, this method is robust as it is insensitive to aerosol characteristics, satellite calibration, or fraction of the image covered by vegetation. Further work by Kaufman (1997) attempted to take advantage of the wide spectral range of the MODIS sensor and identify dark pixels in the mid-infrared wavelengths (2.1 and 3.8 μm), where aerosol optical depth is traditionally

low due to the large wavelength relative to typical aerosol particle size. An estimation of reflectance at visible wavelengths (0.47 and 0.66 μm) was then accomplished. The error in the algorithm for aerosol optical depth (τ) was estimated at $\Delta\tau = \pm 0.05$ to ± 0.2. Uncertainties were related to refractive index, single-scatter albedo, and aerosol characteristics. Also, contamination of the longer wavelengths by dust resulted in an unreliable correlation between the infrared and visible wavelengths.

Hsu *et al* (2004) attempted to solve the challenge in retrieving accurate aerosol properties over bright surfaces. In many regions, such as arid, semi-arid, and urban areas, the surface reflectance is bright in the red and near-infrared wavelengths, but much darker in the blue wavelengths. Hsu developed a method known as "Deep Blue", which uses combinations of blue channel sensors to detect aerosol particles at a much lower aerosol loading. However, variability of dust optical properties is much greater at this end of the spectrum. Therefore, a red channel is used for heavy aerosol loading cases. Research showed this method to be within 20% of ground truth Aerosol Robotic Network (AERONET) values. Uncertainties in the "Deep Blue" method are due to assumptions in the vertical profile of the aerosol, errors in estimation of particle size and shape, and approximations of the surface reflectance due to use of a 0.1° by 0.1° database.

3. Multi-angle Method

A completely different approach to solving this problem was taken by Veefkind *et al* (1998) with what is known as the Multi-angle Method. The Multi-angle Method is only possible with multi-view sensors such as the Along Track Scanning Radiometer (ATSR-2) and the Multi-angle Imaging Spectro Radiometer (MISR), demonstrated by Martonchik *et al* (2004). ATSR-2 utilizes seven wavelength bands, four in the visible bands and three in the infrared bands. There are two viewing angles, nadir and a forward view at a 55° incident angle to the surface. MISR utilizes four wavelength bands and senses from nine viewing angles. These multiple angles allow for near simultaneous observation of the surface through different atmospheric columns. While this method has proven successful, particularly over bright surfaces, there are limited multi-view

capabilities in operation. As well, the revisit times of ATSR-2 and MISR, approximately three and nine days respectively, make real-time, operational AOD retrievals unrealistic.

B. SHADOW METHOD

1. Introduction

New attempts at retrieving AOD measurements over land have been made in the past few years. There have been significant advances in high-resolution commercial satellite imagery available to the public, particularly DigitalGlobe's QuickBird satellite. This high-resolution imagery is now capable of resolving ground features not previously possible, such as clearly defined shadows generated by buildings and clouds. Other sensor platforms, such as ASTER on the TERRA satellite, and MODIS, while not at nearly the resolution of QuickBird, still provide sufficient resolution to distinguish larger scale shadows cast by clouds. The Shadow Method is an effort to address the challenges of measuring AOD over bright surface areas, such as desert regions. Vincent (2006) developed this method and found that AOD retrievals using QuickBird imagery are possible with an error of ±0.04.

2. Shadow Method Summary

Retrieving AOD through commercial satellite imagery is a very recent idea that is only made possible through advances in imagery resolution. The resolution of QuickBird (60-70 centimeter for panchromatic; 2.4 and 2.8 meter for multi-spectral) allows for delineation of buildings such as apartments, towers, and hangars. Shadows can be identified and clearly defined, and a comparison of radiance values inside and directly outside of the shadow over a homogeneous surface is then used to characterize the atmospheric aerosol particles.

There are three main sources of radiation that the sensor detects: direct transmission, diffuse transmission, and diffuse reflection (Vincent 2006). Figure 1 graphically depicts these three sources. Direct transmission is radiation that travels directly from the source (sun) and reflects directly into the sensor. Diffuse transmission is defined as radiation that is reflected off atmospheric constituents (aerosol particles and

gases) down to the reflecting surface then directly to the sensor. Diffuse reflection is radiation that is scattered by atmospheric constituents down to the reflecting surface, back to the atmospheric constituents, back down to the reflecting surface and finally up to the sensor (Evans 2007). The shadow region is comprised of diffuse transmission and diffuse reflection—no direct solar radiation is received. Outside of the shadow region, direct transmission is received along with diffuse reflection and diffuse transmission.

There are benefits to using this method that are not available in other methods. First, retrieval success is independent of wavelength. The Deep Blue technique only retrieves results in the blue wavelengths while the Shadow Method provides results for every available solar channel. Also, the results are independent of shadow generator. As long as the surfaces in and out of the shadow have identical reflectance characteristics, the diffuse transmission and reflection can be isolated to arrive at the direct transmission portion.

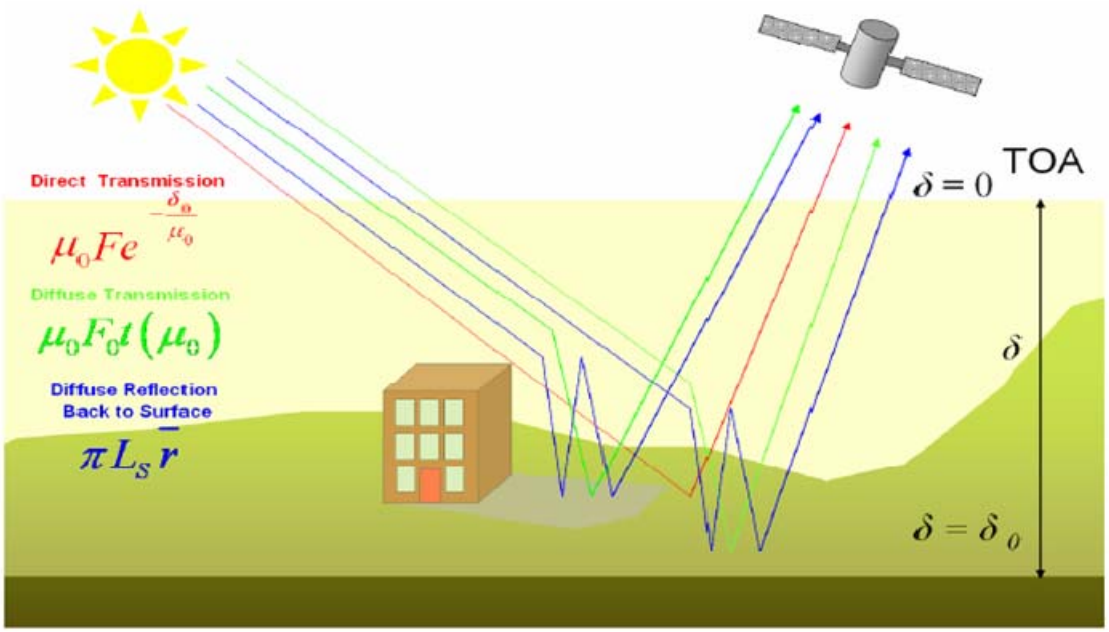

Figure 1. The shadow method uses the difference between the radiances within and outside of the shadowed area to quantify the direct transmission and the total optical depth. Optical depth is defined as the sum of extinction above a vertical position in the atmosphere (therefore equals zero at the top of the atmosphere).Vincent 2006

3. Governing Equation

The governing equation was derived by Vincent (2006) by mathematically defining the three sources of radiation and deriving equations for radiance in the shaded and unshaded regions. Subtracting these two equations and solving for optical depth, δ_0, an equation for determining optical depth is calculated:

$$\delta_0 = \left(\frac{\mu_0 \mu}{\mu + \mu_0} \right) \ln \left[\left(\frac{r_s}{1 - r_s \bar{r}} \right) \left(\frac{\mu_0 F_0}{\pi L_d} \right) \right]$$

This equation is the governing equation for solving optical depth by measuring radiance values inside and outside of shadow regions over a homogeneous surface.

All terms except for mean aerosol reflectance, $\bar{r}$, are known. This term is assumed to be much smaller than the surface reflectance such that the product of the two in the equation above results in a value much less than one. The total optical depth is then corrected for molecular Rayleigh scattering. Vincent (2006) determined the Rayleigh optical depth based on the work of Russell *et al* (1993) and Frolich and Shaw (1980). The Rayleigh optical depths for QuickBird, MODIS, ASTER, and IKONOS are depicted in the following tables.

Table 1. Molecular Rayleigh optical depths for each of the QuickBird channels assuming a radiometer height of zero kilometers and atmospheric pressure of 1013.25 hPa. (Vincent 2006)

Band	**Center Effective Wavelength (micrometers)**	**Molecular Rayleigh Optical Depth**
Panchromatic	0.673	0.05
Blue	0.482	0.17
Green	0.556	0.09
Red	0.658	0.05
Near-Infrared	0.816	0.02

Table 2. Molecular Rayleigh optical depths for each of the MODIS channels assuming a radiometer height of zero kilometers and atmospheric pressure of 1013.25 hPa.

Band	**Center Effective Wavelength (micrometers)**	**Molecular Rayleigh Optical Depth**
Blue	0.469	0.19
Green	0.556	0.09
Red	0.645	0.05
Near-Infrared	0.853	0.02
Short-Wave Infrared	1.640	0

Table 3. Molecular Rayleigh optical depths for each of the ASTER channels assuming a radiometer height of zero kilometers and atmospheric pressure of 1013.25 hPa.

Band	**Center Effective Wavelength (micrometers)**	**Molecular Rayleigh Optical Depth**
Green	0.556	0.09
Red	0.661	0.05
Near-Infrared	0.807	0.02

Table 4. Molecular Rayleigh optical depths for each of the IKONOS channels assuming a radiometer height of zero kilometers and atmospheric pressure of 1013.25 hPa.

Band	**Center Effective Wavelength (micrometers)**	**Molecular Rayleigh Optical Depth**
Panchromatic	0.727	0.03
Blue	0.480	0.17
Green	0.551	0.10
Red	0.665	0.05
Near-Infrared	0.805	0.02

THIS PAGE INTENTIONALLY LEFT BLANK

III. DATA AND METHODOLOGY

A. DATA

1. Location

All case studies in this thesis focused on Southwest Asia, specifically Saudi Arabia and the United Arab Emirates. This was done for two reasons. First, as stated in Chapter II, all previous methods of determining aerosol optical depth have had difficulty over bright backgrounds. The Arabian Desert provides the bright background necessary to test the Shadow Method. Second, this region has been the focus of military operations for over 17 years. If this method is going to be applied operationally, it needs to be tested and verified in this region. To apply the Shadow Method to cloud shadows, cumulus clouds are ideal as they generally provide shadows with more clearly defined edges than middle and upper clouds. Also, cumulus clouds, particularly in this region, are associated with unstable air, often with multiple clouds whose shadows can be sampled. Figures 2-5 below depict typical months in winter, spring, summer, and fall with frequency of occurrence of cumulus clouds. January through May provides the greatest chance for cumulus cloud development, with the second half of the year decreasing in frequency.

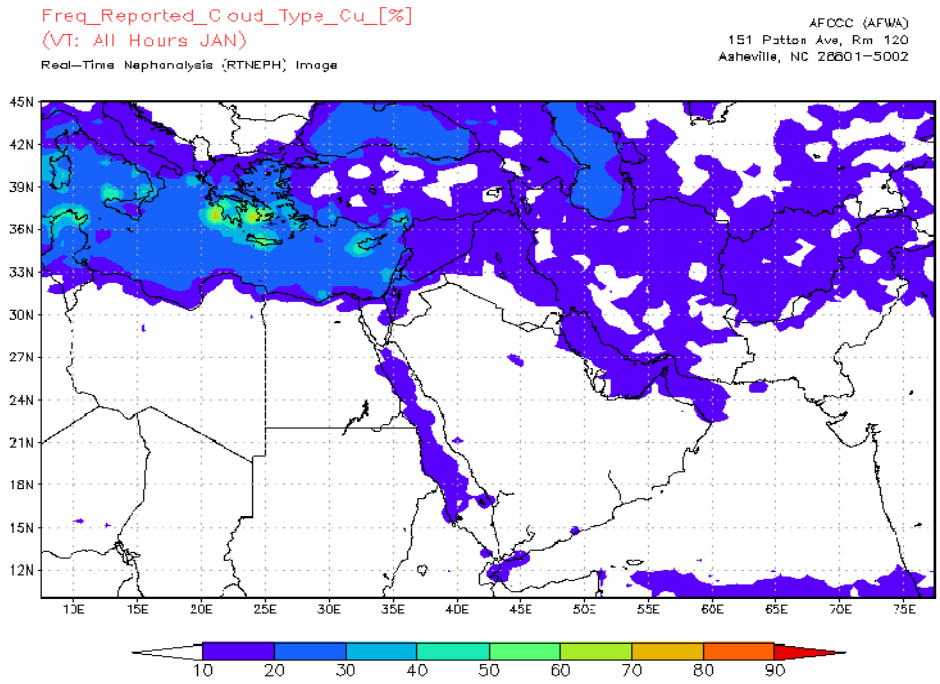

Figure 2. Frequency of occurrence of cumulus clouds over Southwest Asia in January (Air Force Combat Climatology Center 2008).

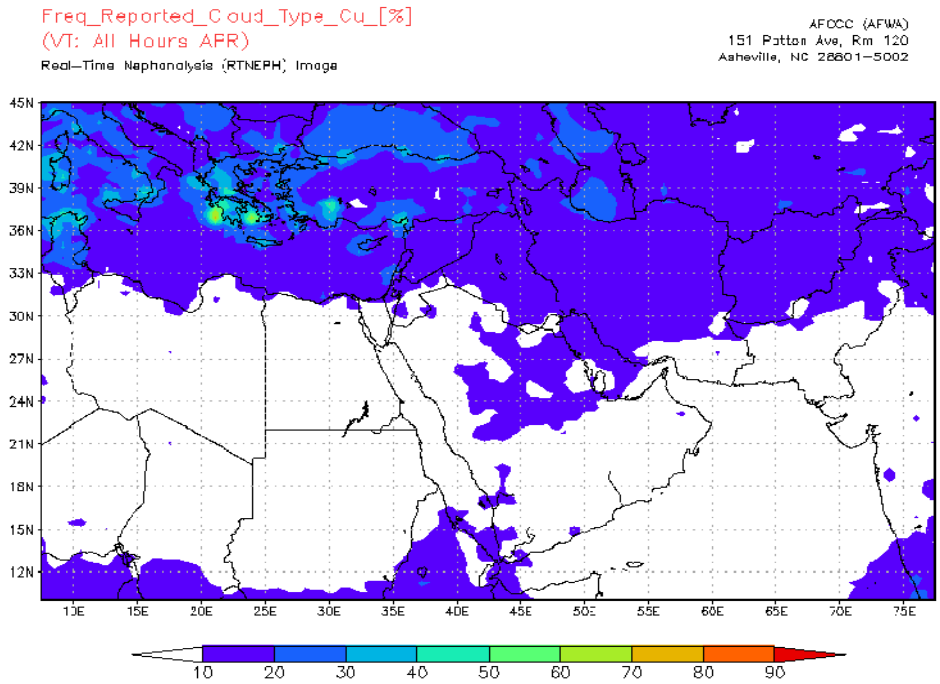

Figure 3. Frequency of occurrence of cumulus clouds over Southwest Asia in April (Air Force Combat Climatology Center 2008).

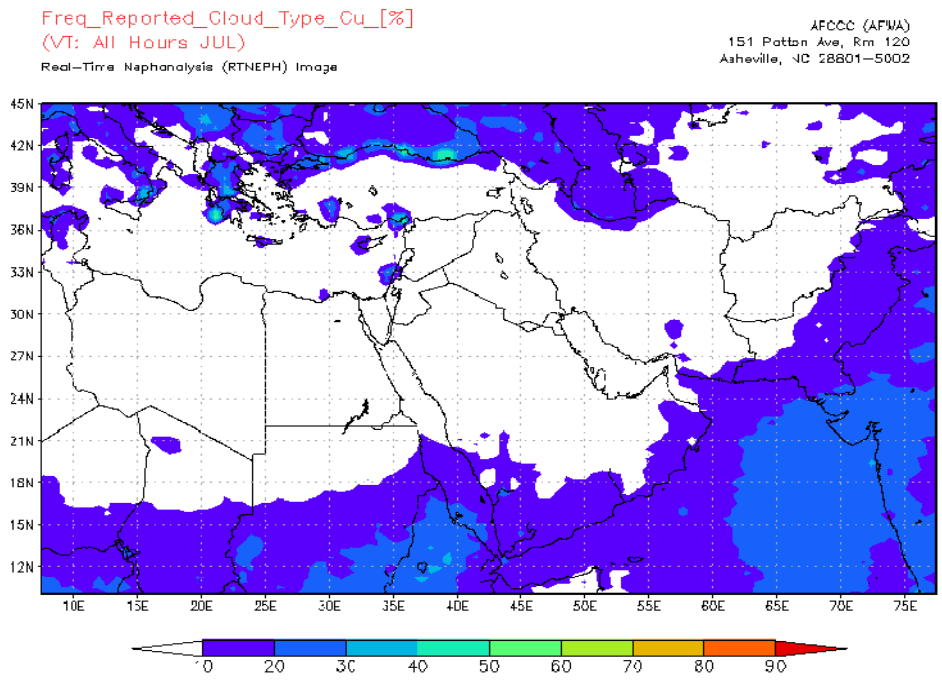

Figure 4. Frequency of occurrence of cumulus clouds over Southwest Asia in July (Air Force Combat Climatology Center 2008).

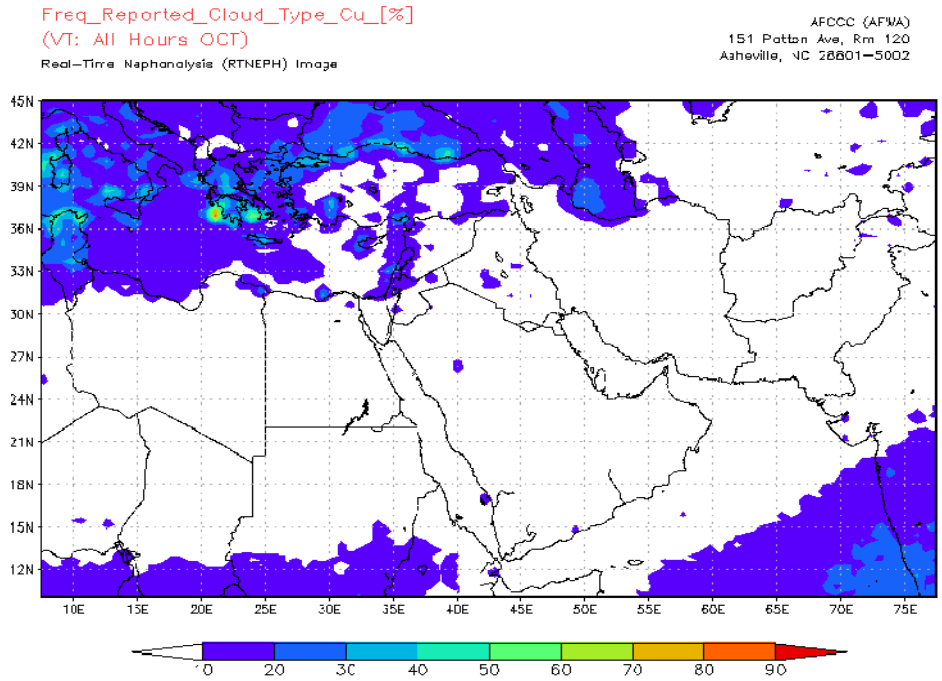

Figure 5. Frequency of occurrence of cumulus clouds over Southwest Asia in October (Air Force Combat Climatology Center 2008).

2. QuickBird

QuickBird imagery has been solely used for the shadow technique until this study. The satellite was launched in 2001 and operates at an altitude of 450 kilometers at a 98° sun-synchronous inclination angle. This allows for a revisit frequency of approximately one day at the poles and closer to 3.5 days near the equator. The satellite crosses the equator at 1030 local time and the swath width is 16.5 km. QuickBird provides imagery at two different resolutions: 0.61 meter resolution from the panchromatic sensor (445 nm to 900 nm) and 2.44 meter resolution from the multi-spectral sensor. The multi-spectral sensor consists of a blue (450 nm to 520 nm), green (520 nm to 600 nm), red (630 nm to 690 nm), and near-infrared (760 nm to 900 nm) channel. (DigitalGlobe 2008)

3. MODIS

A goal of this thesis is to study how effective this technique is with sensors at lower resolutions than QuickBird. One of these sensors is MODIS, located on both the Terra and Aqua satellites. These satellites operate at an altitude of 705 km and are positioned so that Terra descends over the equator at 1030 local time while Aqua ascends over the equator at 1330 local time. They operate in a sun-synchronous orbit with an inclination angle of 98.2° and combined can view the entire Earth every 1-2 days. MODIS operates at a ±55° scanning pattern which results in a swath width of 2330 km, noticeably different than that of QuickBird. MODIS provides imagery in 36 spectral bands ranging from 400 nm to 1440 nm in wavelength. Three different resolutions are available depending on the band. Bands 1 and 2 are available at 250 meter resolution, Bands 3-7 are available at 500 meter resolution, and Bands 8-36 are available at 1000 meter resolution. The table below shows the bands and their respective channel used for this study (GSFC 2008).

Table 5. MODIS bandwidths with respective channel and resolution used in this study.

Band	Bandwidth (nm)	Channel	Resolution (m)
1	620-670	Red	250
2	841-876	Near-Infrared	250
3	459-479	Blue	500
4	545-565	Green	500
6	1628-1652	SWIR	500

4. ASTER

ASTER, like MODIS, is an imaging radiometer flown on Terra and therefore operates with the same orbit characteristics as MODIS. ASTER has a swath width of 60 km and has a revisit time of 16 days. Imagery is provided in 14 different bandwidths ranging from 520 nm to 11.65 μm. Three different ground resolutions are available. Bands 1-3 (Very Near-Infrared) provide imagery at 15 meter resolution, Bands 4-9 (Short Wave Infrared) provide imagery at 30 meter resolution, and Bands 10-14 (Thermal Infrared) provide 90 meter resolution imagery. The table below shows bands and respective bandwidths used in this study (JPL 2008).

Table 6. ASTER bandwidths with respective channel and resolution used in this study.

Band	Bandwidth (nm)	Channel	Resolution (m)
1	520-600	Green	15
2	630-690	Red	15
3	760-860	Near-Infrared	15

5. IKONOS

IKONOS is a high-resolution satellite very similar to QuickBird. It was launched in 1999 and provided the first one-meter resolution imagery from a commercial satellite.

It operates at an orbit of 681 kilometers in a sun-synchronous orbit with an inclination angle of 98.1°**.** IKONOS has a revisit time of approximately three days at 40° latitude**.** Like QuickBird, IKONOS provides imagery in blue, green, red, near-infrared, and panchromatic bandwidths. At nadir, panchromatic imagery is provided at 0.82 meter resolution. All other channels are provided at 3.2 meter resolution. The swath width of IKONOS is 11.3 km at nadir. (GEOEYE 2008)

6. AERONET

AERONET readings were used as ground truth for the Shadow Method for the three instruments. The AERONET program is a ground-based remote sensing network established by NASA, the French National Center for Scientific Research (CNRS), and other agencies and universities. This network provides observations of AOD, inversion products, and diverse aerosol regimes from around the globe. Three different levels of data are provided: Level 1.0 (unscreened), Level 1.5 (cloud-screened), and Level 2.0 (cloud-screened and calibrated). AERONET retrievals are taken at the center wavelengths and bandwidths listed in the table below. For this study, 440, 675, 870, 1020, and 1640 nm wavelengths were used.

Table 7. Standard AERONET Channels and their associated bandwidths (GSFC 2008).

Standard AERONET Wavelengths (nm)	Bandwidth (nm)
340	2
380	4
440	10
500	10
675	10
870	10
940	10
1020	10
1640	25

AERONET instruments are recalibrated every six to twelve months and analyses show an uncertainty of approximately 0.01 to 0.02 in AOD due to calibration methods (GSFC 2008).

B. METHODOLOGY

The Environment for Visualizing Images (ENVI) 4.3 software was used for viewing, georeferencing, orthorectificating, calibrating, and analyzing all imagery in this study. Code written by Dombrock (2007) in the Interactive Data Language (IDL) was used to calculate optical depths according to the governing equation. Since there were three types of imagery studied, analysis varied according to the imagery interrogated as described below.

1. Imagery Collection

The QuickBird, IKONOS, and ASTER imagery used in this investigation were obtained through the National Geospatial-Intelligence Agency via the Commercial Satellite Imagery Library. MODIS imagery was obtained through NASA's Level 1 and Atmospheric Archive Distribution System (LAADS).

There were several factors that had to be accounted for before choosing suitable imagery. First, there must be an AERONET site available in the region with current optical depth measurements. Also, samples taken from imagery must be considered representative of measurements at the AERONET site. A defined range from the AERONET location was not specified due to inconsistencies in available samples and the differing resolutions of the imagery. Representativeness was done subjectively by analyzing the synoptic pattern of the region. There also needed to be sufficient shadows generated by clouds. Since all satellites in this study are in a sun-synchronous orbit, shadow size in a particular image was strictly dependent on the height and thickness of clouds. Shadows at resolutions near or below the image resolution were considered unreliable and not considered. Finally, shadows had to be over a bright and homogeneous background. Shadows that fell over complicated surfaces such as mountain ranges or over dark backgrounds were not considered.

2. Imagery Orthorectification

For the QuickBird imagery used, images were orthorectified to project image coordinates into real-world coordinates that allow for corrections in tilt and relief. ENVI allows the user the choice of orthorectifying using a rational polynomial coefficient (RPC) file provided with the imagery or defining ground control points in the imagery. The RPC file was used for this purpose for all QuickBird imagery.

3. Imagery Georeferencing

The MODIS and ASTER imagery used in this study was provided with header information that included latitude and longitude of any point in the image. However, it does not arrive preprocessed in this manner. ENVI was used to extract latitude and longitude values from the header information to georeference the data. This information was necessary to determine exactly where the AERONET collection site was in the image and determine distances from this location.

4. Conversion to Calibrated Absolute Radiance/At-Sensor Radiance Values

The QuickBird imagery was calibrated for absolute radiance after orthorectification. Vincent (2006) constructed an expression based on the absolute calibration factor and bandpass width for each channel to alleviate potential errors in using the ENVI-provided calibration tool. This expression reduces the uncertainty in the absolute radiance values that is introduced by rounding off bandpass width values.

IKONOS imagery is provided with values in a Digital Number format and conversion to at-sensor radiance is necessary. The Band Math tool in ENVI was used to apply the equation below and determine radiance values.

$$L_\lambda = 10^4 * DN_\lambda / CalCoef_\lambda * Bandwidth_\lambda$$

L_λ is the radiance for the spectral band λ at the sensor, DN is the Digital Number provided in the IKONOS imagery, CalCoef is the radiometric calibration coefficient, and Bandwidth is the bandwidth of the spectral band. The table below outlines the CalCoef and Bandwidth for each spectral band.

Table 8. Calibration Coefficients and Bandwidth for each spectral band in IKONOS imagery (GEOEYE 2008).

IKONOS Band	CalCoef ($DN / mW / cm^2 - sr$)	Bandwidth (nm)
Panchromatic	161	403
Blue	728	71.3
Green	727	88.6
Red	949	65.8
NIR	843	95.4

5. Sample Retrieval

Sampling was performed using ENVI's Region of Interest (ROI) tool. This tool allows the user to define a polygon, rectangle, or line and analyze data in that area only. One sample was taken inside the shadow and the second sample was taken directly outside the shadow. Care was taken to ensure there was clear delineation of where the shadow ended. Also, it was critical to guarantee the background was reasonably homogeneous. This step was easier to verify with QuickBird, IKONOS, and ASTER imagery than it was with MODIS imagery at 500 meter resolution.

6. Determination of Aerosol Optical Depth

Aerosol optical depths were extracted through an IDL program developed by Vincent (2006) and further modified by Dombrock (2007) to automate radiance extraction from ENVI. User input was required for satellite zenith angle, solar zenith angle, and estimate of single scatter albedo and asymmetry parameter; which were retrieved from file header and climatology information. Optical depth results were output with a maximum, mean, and minimum measurement. The mean result was used in all case studies.

7. Analysis

An analysis of the ground truth data from the AERONET sun photometers was required before shadow samples were taken. The tables below detail the wavelengths used for each of the satellite instruments. Since these do not match the AERONET channels, the AERONET data was applied to an exponential best-fit curve. An example is shown in Figure 6. This was required for every change in imagery (scene and/or instrument).

Table 9. QuickBird minimum, maximum and center effective wavelengths (after DigitalGlobe (2005)) with in band spectral solar irradiance based on Wehrli (1985) spectral solar irradiance curves.

QuickBird Channel	Minimum Wavelength (nm)	Maximum Wavelength (nm)	Center Effective Wavelength (nm)	Spectral Solar Irradiance ($W\ m^{-2}\ nm^{-1}$)
Ch 1 (Blue)	450	520	482	1973
Ch 2 (Green)	520	600	556	1854
Ch 3 (Red)	630	690	658	1570
Ch 4 (Near-Infrared)	760	900	816	1095
Panchromatic	445	900	673	1506

Table 10. IKONOS minimum, maximum and center effective wavelengths (after GEOEYE (2007)) with in band spectral solar irradiance based on Wehrli (1985) spectral solar irradiance curves.

IKONOS Channel	Minimum Wavelength (nm)	Maximum Wavelength (nm)	Center Effective Wavelength (nm)	Spectral Solar Irradiance ($W\ m^{-2}\ nm^{-1}$)
Ch 1 (Blue)	445	516	480	1880
Ch 2 (Green)	506	595	551	1870
Ch 3 (Red)	632	698	665	1535
Ch 4 (Near-Infrared)	757	853	805	1111
Panchromatic	526	929	727	1382

Table 11. MODIS minimum, maximum and center effective wavelengths with in band spectral solar irradiance based on Wehrli (1985) spectral solar irradiance curves.

MODIS Channel	Minimum Wavelength (nm)	Maximum Wavelength (nm)	Center Effective Wavelength (nm)	Spectral Solar Irradiance (W m^{-2} nm^{-1})
Ch 1 (Red)	620	670	645	1628
Ch 2 (Near-Infrared)	841	876	858	1014
Ch 3 (Blue)	459	479	469	2018
Ch 4 (Green)	545	565	555	1860
Ch 6 (Shortwave-Infrared)	1628	1652	1640	234

Table 12. ASTER minimum, maximum and center effective wavelengths with in band spectral solar irradiance based on Wehrli (1985) spectral solar irradiance curves.

ASTER Channel	Minimum Wavelength (nm)	Maximum Wavelength (nm)	Center Effective Wavelength (nm)	Spectral Solar Irradiance (W m^{-2} nm^{-1})
Ch 1 (Green)	520	600	560	1861
Ch 2 (Red)	630	690	660	1573
Ch 3 (Near-Infrared)	760	860	810	1121

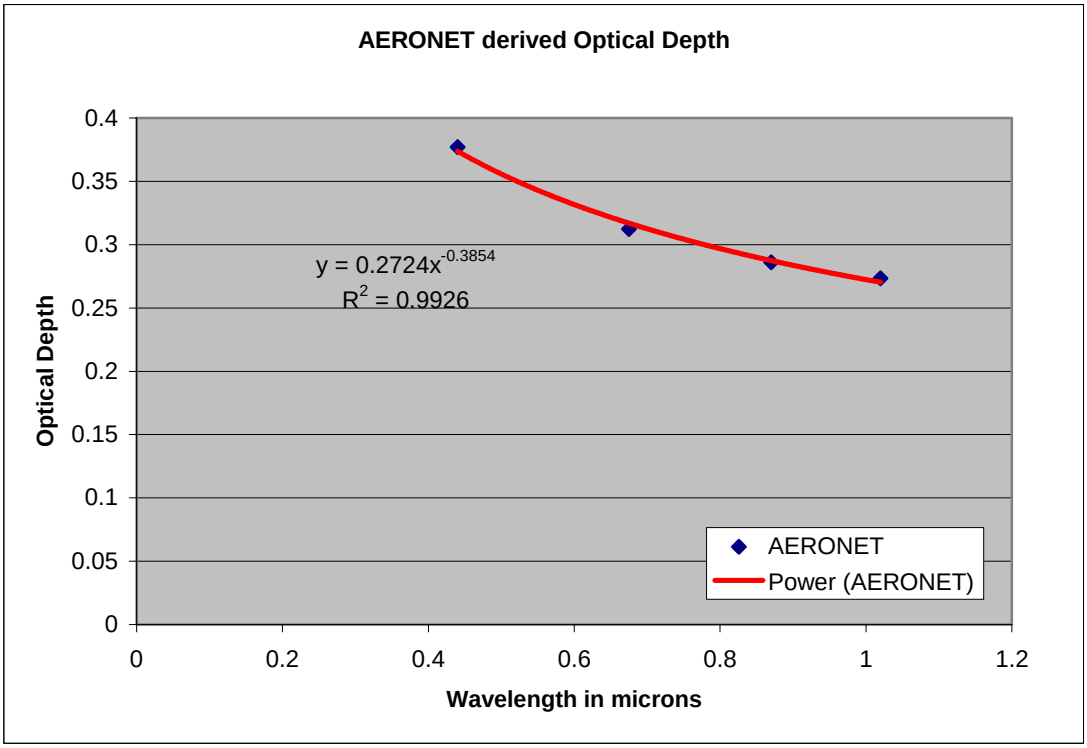

Figure 6. Sample best-fit curve applied to extract equivalent AERONET derived optical depth.

Once the equivalent AERONET measurements were determined, the results from the Shadow Method were analyzed and compared to these values. Evans (2007) determined that using the mean radiance value from the shaded region in the calculation was more accurate than the minimum radiance value over urban areas due to possible influence from surface variations. Factors that influenced the final results varied according the instrument used. The background sampled should be as homogeneous as possible as mentioned in Chapter II. QuickBird, ASTER, and IKONOS imagery backgrounds were considered acceptable to judge the background due to the higher resolutions. However, at such high resolutions, an extraneous amount of background detail can be deciphered, making the decision of where to sample difficult. In these cases, it was imperative to ensure the background in both the shaded and unshaded areas were as close as possible. MODIS imagery is at much lower resolution and therefore the background lacks detail and generally appears homogenous.

The resolution of the QuickBird and IKONOS imagery introduced another factor when analyzing cloud shadows. Previous studies focused on building shadows. In these cases, the shadow can receive indirect radiation from reflectors such as buildings (Evans 2007). When studying cloud shadows, additional indirect radiation is received around the edges of the shadow due to the cloud being suspended above the ground. As a result, there is more diffusivity around the edge of the cloud shadow than a building shadow. This effect is shown in Figure 7. Three samples were taken at various locations within the cloud shadow and compared to the same surface outside the shadow. Optical depth calculations varied by as much as 0.5 although all samples were considered within the shadow.

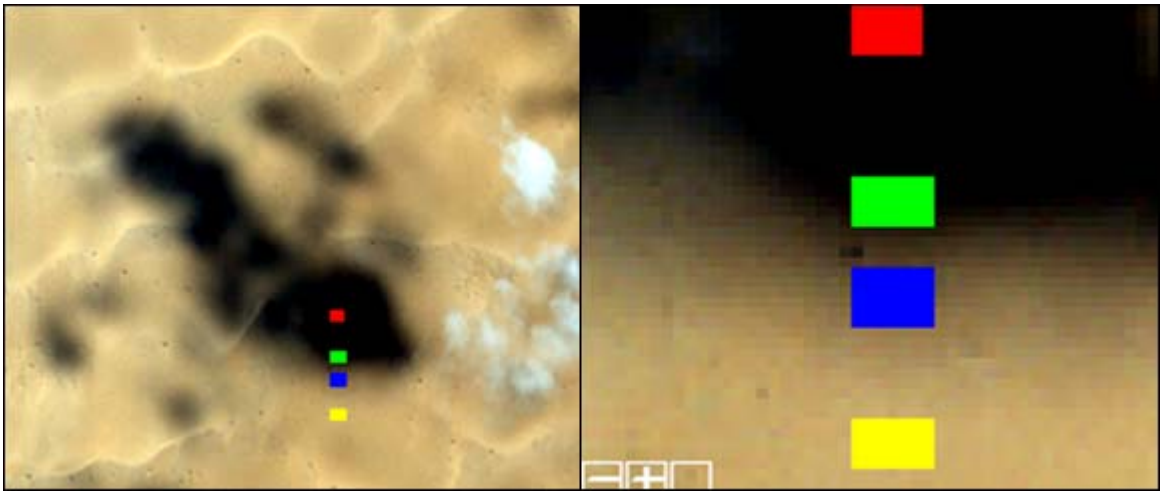

Figure 7. IKONOS imagery of cloud shadow. The image on left displays the full cloud shadow. The image on right illustrates the samples taken more clearly. Note how cloud shadow edge becomes blurred, requiring sample selections to be made carefully. Colored boxes denote where samples were taken in Table 13.

Table 13. Measured optical depths for the blue, green, red, and near-infrared channels from different regions within same cloud shadow. All three shaded samples were compared to the same unshaded sample, which is yellow.

Shaded Sample Location	Blue Channel	Green Channel	Red Channel	Near Infrared Channel
Red	0.5360	0.4431	0.3900	0.3458
Green	0.6202	0.5235	0.4664	0.4198
Blue	0.9761	0.8747	0.8297	0.7814

THIS PAGE INTENTIONALLY LEFT BLANK

IV. RESULTS

A. QUICKBIRD—19 SEPTEMBER 2004

1. Overview

Imagery used from QuickBird was collected over the island of Sir Bu Nair off the United Arab Emirates (UAE) coast on 19 September 2004. Three different images were captured during the pass: forward-looking, approximately nadir, and a rear-looking image. Figure 8 displays an overview of the region for this day. Figures 9-11 display the QuickBird images from forward, nadir, and rear angles, respectively. Two primary cloud shadows were sampled and then compared to measurements from an AERONET site located on island.

Table 14. Time of QuickBird passes over Sir Bu Nair along with satellite and solar zenith angles for each collection.

Location	Date	Time (UTC)	Satellite Zenith	Solar Zenith
Sir Bu Nair	19 Sep 04	0651	54.1	31.4
Sir Bu Nair	19 Sep 04	0653	34.1	31.2
Sir Bu Nair	19 Sep 04	0654	54.7	31.0

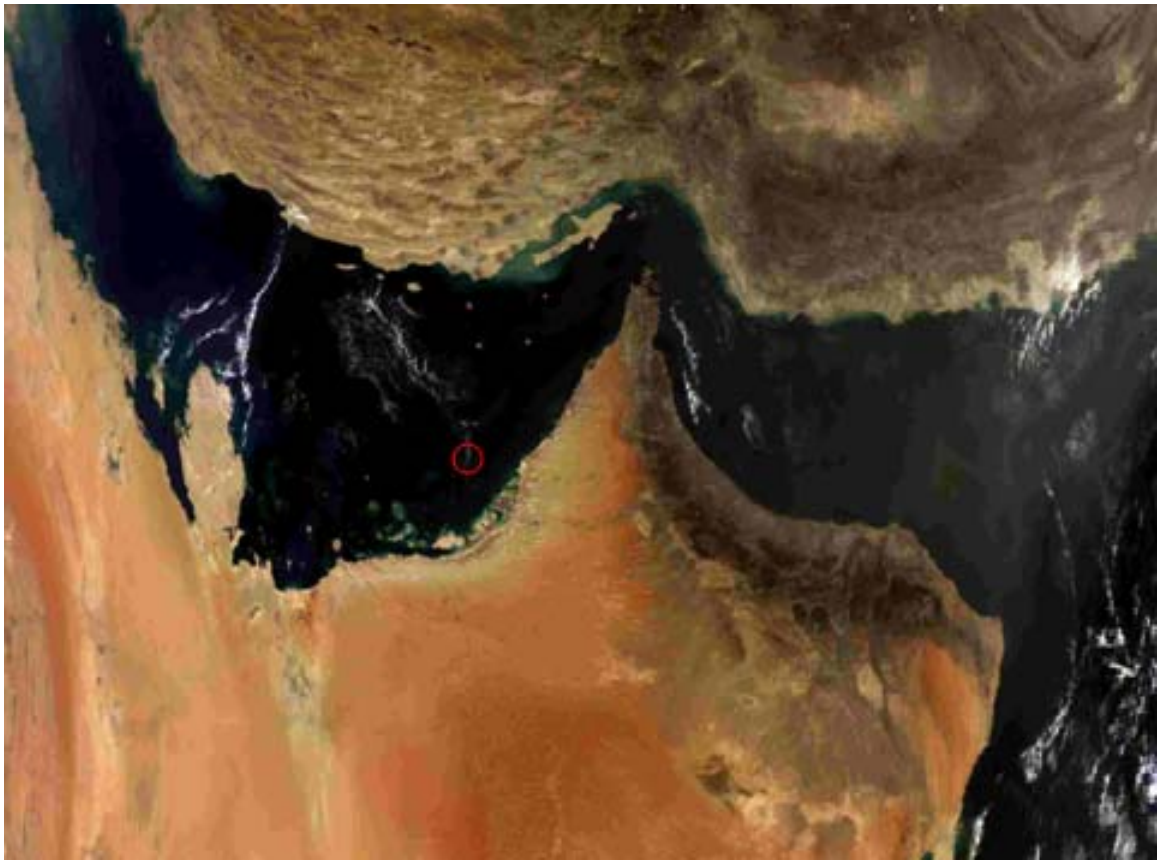

Figure 8. MODIS overview of southeastern Saudi Arabia and United Arab Emirates for 19 September 2004. Red circle denotes location of Sir Bu Nair.

Figure 9. Forward-looking image of Sir Bu Nair from QuickBird collected on 19 September 04.

Figure 10. Image of Sir Bu Nair from QuickBird at approximately nadir collected on 19 September 04.

Figure 11. Rear-looking image of Sir Bu Nair from QuickBird collected on 19 September 04.

2. Ground Truth

The ground truth optical depth was retrieved from the AERONET site and the equivalent QuickBird channels were then derived. The table below depicts the derived AERONET values that were used for verification.

Table 15. AERONET integrated AOD for 19 September 2004 over Sir Bu Nair.

Channel	Blue	Green	Red	NIR	Panchromatic
Band(microns)	0.450-0.520	0.520-0.600	0.630-0.690	0.760-0.900	0.445-0.900
AOD	0.4975	0.4359	0.3777	0.3327	0.3774

3. Results

a. Forward-looking

The set of data in Table 16 shows results from the forward-looking image collection. Eight samples were taken from each image. The average AOD and standard

deviation are shown in the first table below. Table 17 displays the values of all samples taken along with distance from the AERONET site. All samples were taken within approximately three miles of the AERONET sensor. Figure 12 illustrates how well the shadow method correlated to AERONET measurements. The results were fairly consistent with a slightly low bias across all wavelengths. Although the panchromatic channel had an effective wavelength of 673 nm, which is very close to the red channel (658 nm), the panchromatic results were much closer to AERONET readings. This is most likely due to the quality of the panchromatic imagery and the ability to take confident samples inside and outside of the shadow.

Table 16. Shadow Method AOD results for forward-looking angle over Sir Bu Nair.

Channel	Blue	Green	Red	NIR	Panchromatic
Average	0.4918	0.3922	0.2949	0.2578	0.3552
Standard Deviation	0.0552	0.0475	0.0472	0.0446	0.0414

Table 17. Table showing sample values and distance from AERONET site used for representativeness of forward-looking angle.

Distance (km)	Blue	Green	Red	NIR	Panchromatic
3.1	0.426378	0.334789	0.244826	0.218874	0.316723
2.9	0.541363	0.392434	0.28076	0.245375	0.311277
2.5	0.469896	0.36881	0.262089	0.224131	0.309529
3	0.410886	0.326731	0.24117	0.2079	0.418212
2.1	0.513852	0.406352	0.302007	0.253348	0.384966
1.4	0.478059	0.411138	0.326965	0.287915	0.365687
3.2	0.527339	0.429542	0.322689	0.283002	0.342343
2.6	0.566819	0.468054	0.379007	0.341779	0.392801

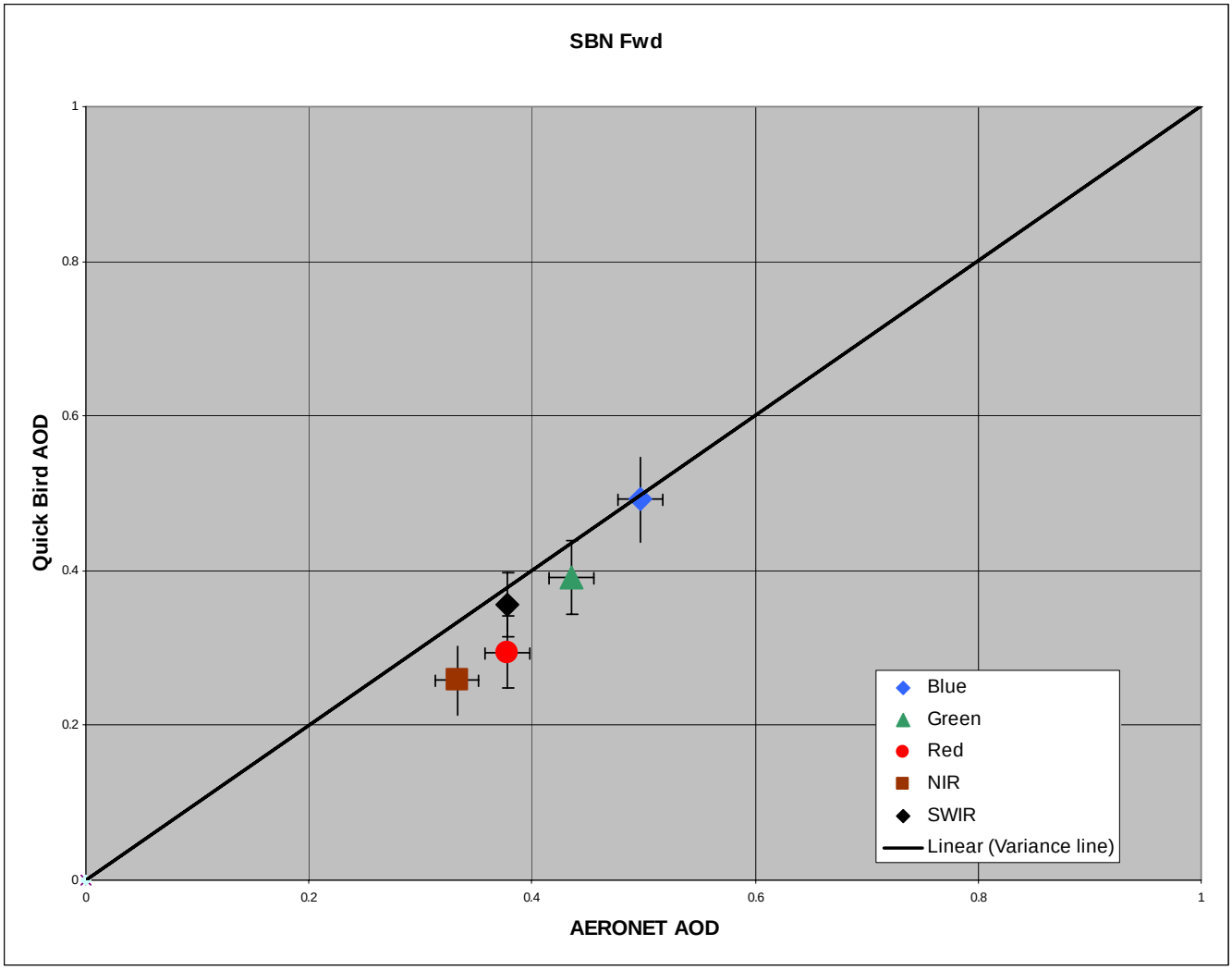

Figure 12. Comparison of QuickBird AOD measurements to AERONET derived AOD measurements over Sir Bu Nair island from a forward-looking angle. The standard error of the samples is annotated as a vertical error bar. The uncertainty of the AERONET measurement, ±0.2, is annotated as a horizontal error bar.

b. Nadir-looking

Table 18 displays the results from samples made from the nadir-looking collection. Ten samples were taken around the cloud shadow. Table 19 displays the values of all samples taken along with distance from the AERONET site. Looking at

Figure 13, the results in this case were slightly lower than the forward-looking case, with the blue and green channels differing the most (0.07 and 0.05, respectively). Again, the slight low bias is apparent.

Table 18. Shadow Method AOD results for nadir-looking angle over Sir Bu Nair.

Channel	Blue	Green	Red	NIR	Panchromatic
Average	0.4204	0.3465	0.2758	0.2528	0.3169
Standard Deviation	0.0617	0.0510	0.0334	0.0299	0.0255

Table 19. Table showing sample values and distance from AERONET site used for representativeness of nadir-looking angle.

Distance (km)	Blue	Green	Red	NIR	Panchromatic
1.3	0.399913	0.323546	0.265974	0.240989	0.289284
2.9	0.453548	0.373747	0.305602	0.285372	0.318942
3	0.371372	0.301809	0.226841	0.201039	0.366074
1.8	0.354242	0.288631	0.238847	0.226498	0.3099
1.4	0.372763	0.314492	0.257938	0.239957	0.321988
3.3	0.34856	0.283995	0.24198	0.226085	0.304982
1.7	0.513072	0.418567	0.318302	0.284733	0.288893
1.8	0.507732	0.418243	0.309459	0.282707	0.355205
3.1	0.468124	0.382705	0.298752	0.266301	0.308031
1.3	0.414611	0.359708	0.294768	0.274647	0.30531

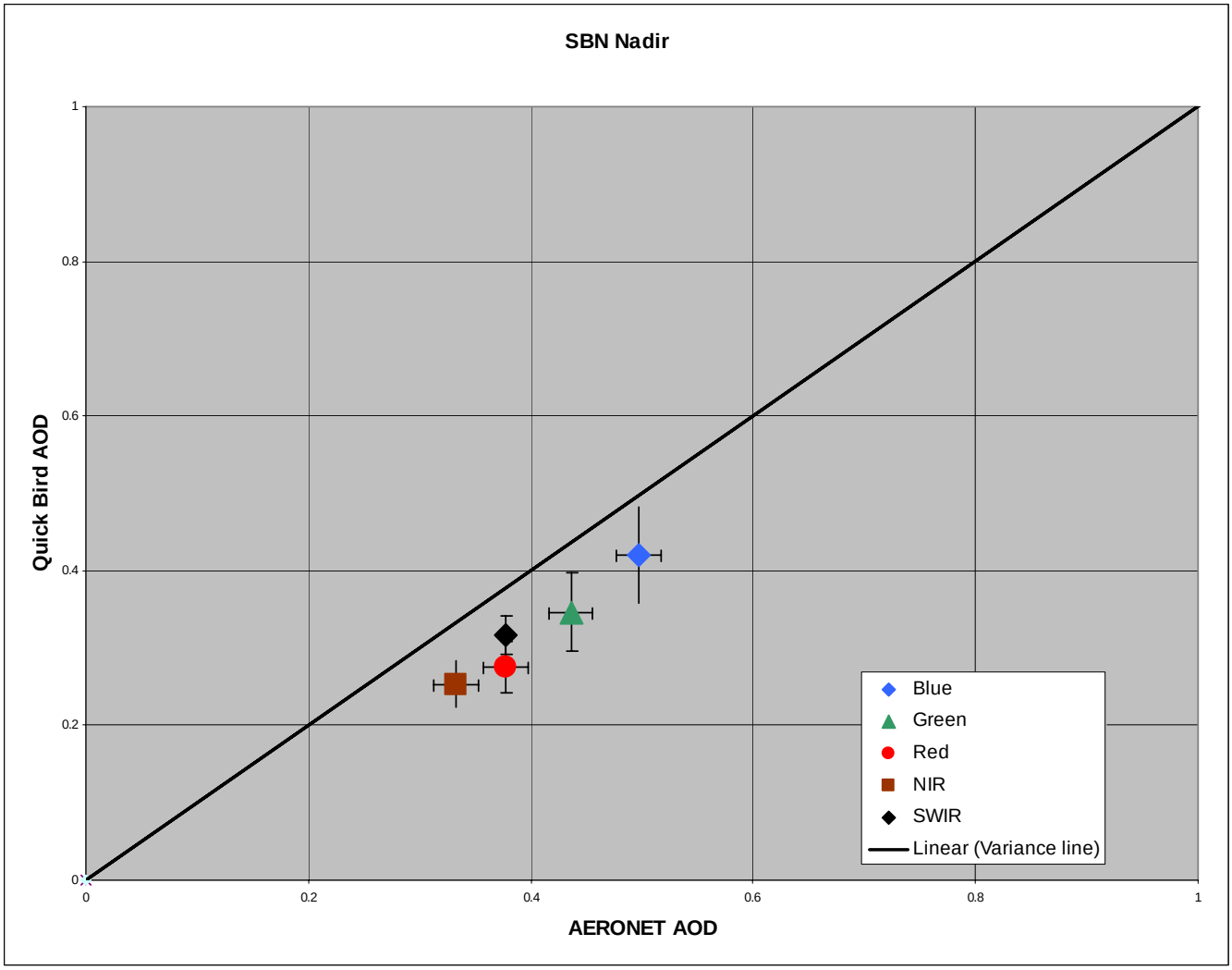

Figure 13. Comparison of QuickBird AOD measurements to AERONET derived AOD measurements over Sir Bu Nair from a nadir-looking angle. The standard error of the samples is annotated as a vertical error bar. The uncertainty of the AERONET measurement, ±0.2, is annotated as a horizontal error bar.

c. Rear-looking

The final results from the QuickBird pass are shown below in Table 20 and Figure 14. Ten samples were taken around the cloud shadow. Table 21 displays the values of all samples taken along with distance from the AERONET site. The results in this case were very similar to the forward-looking angle, with the blue and panchromatic correlating very well to the AERONET values and all channels having a low bias.

Table 20. Shadow Method AOD results for rear-looking angle over Sir Bu Nair.

Channel	Blue	Green	Red	NIR	Panchromatic
Average	0.4892	0.388	0.2809	0.2493	0.3585
Standard Deviation	0.0744	0.0623	0.0424	0.0362	0.0589

Table 21. Table showing sample values and distance from AERONET site used for representativeness of rear-looking angle.

Distance (km)	Blue	Green	Red	NIR	Panchromatic
2.8	0.455769	0.366584	0.267635	0.235972	0.293676
3.8	0.463507	0.355861	0.252852	0.223962	0.373842
2.7	0.483433	0.404873	0.288491	0.257365	0.306879
1.7	0.456991	0.369676	0.297682	0.268731	0.325835
3.2	0.505648	0.399802	0.287507	0.254497	0.325428
3.8	0.520684	0.38781	0.2813	0.241543	0.370077
2.1	0.681647	0.554041	0.388684	0.340416	0.36166
2.8	0.408421	0.341284	0.252424	0.23075	0.505271
3.5	0.46771	0.355749	0.241216	0.213192	0.348646
3.8	0.44832	0.344489	0.251767	0.226245	0.374071

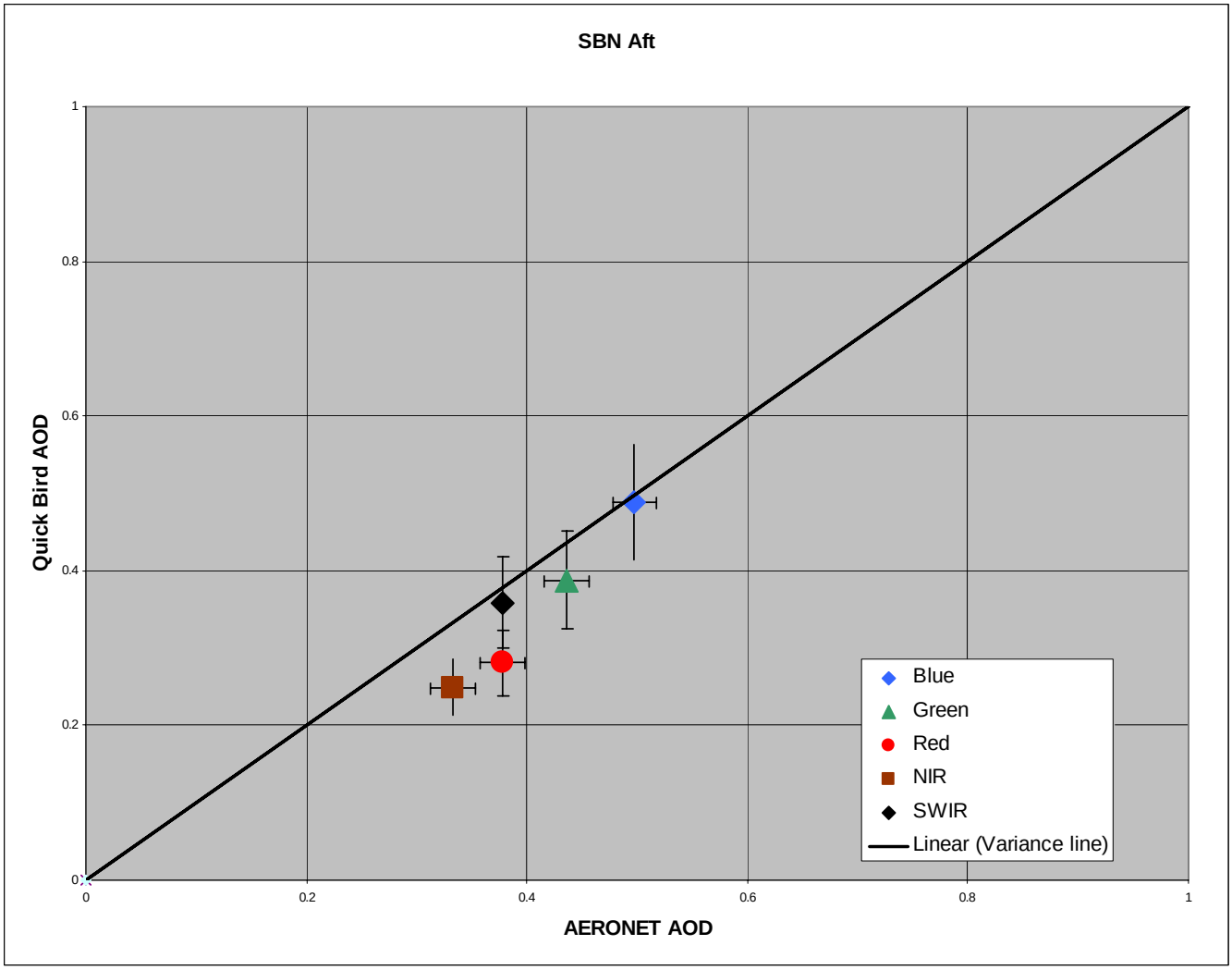

Figure 14. Comparison of QuickBird AOD measurements to AERONET derived AOD measurements over Sir Bu Nair island from a rear-looking angle. The standard error of the samples is annotated as a vertical error bar. The uncertainty of the AERONET measurement, ±0.2, is annotated as a horizontal error bar.

4. Summary

All three angles provided similar results at every wavelength, with slightly lower biases at nadir than forward and aft angles in the blue channel. The results appear to be nearly independent of sensor angle. This slight low bias is consistent with previous case studies sampling QuickBird imagery. Also, Evans (2007) noted how standard deviation decreases with increasing wavelength. Results will be more consistent with longer

wavelengths. This can be attributed to the affect of Rayleigh scattering on each wavelength. As the wavelength increases, the affect of Rayleigh scattering decreases. This relationship holds true in the Sir Bu Nair case as well.

B. ASTER

1. Overview

Contrails were visible in ASTER and MODIS imagery over Saudi Arabia from 15 November 2001 as shown in Figures 15 and 16. These contrails were between 25000 and 30000 feet and provided excellent shadows for sampling along with other cloud shadows in the image.

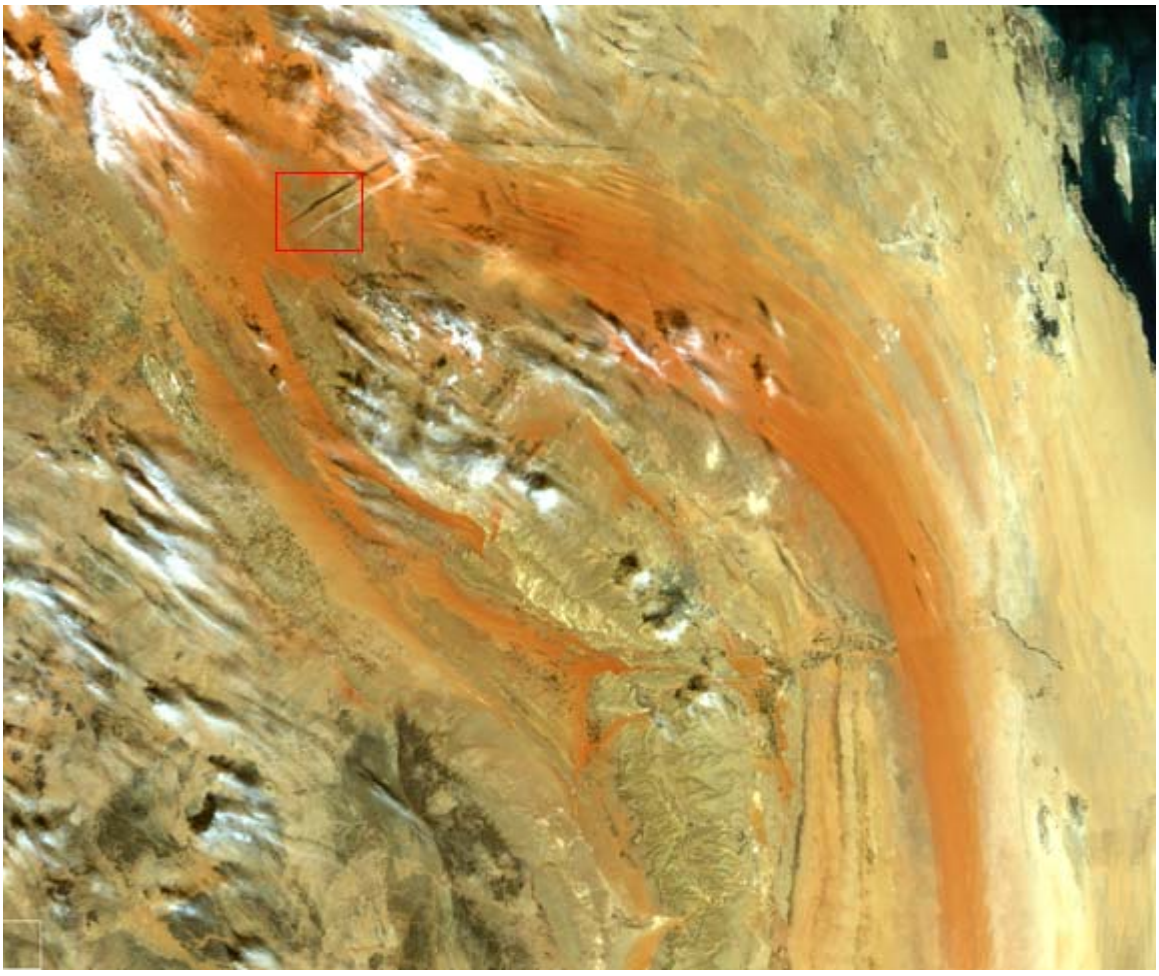

Figure 15. MODIS overview of Saudi Arabia for 15 November 2001. Red circle denotes location of Solar Village AERONET site. Red box denotes dimensions of ASTER imagery.

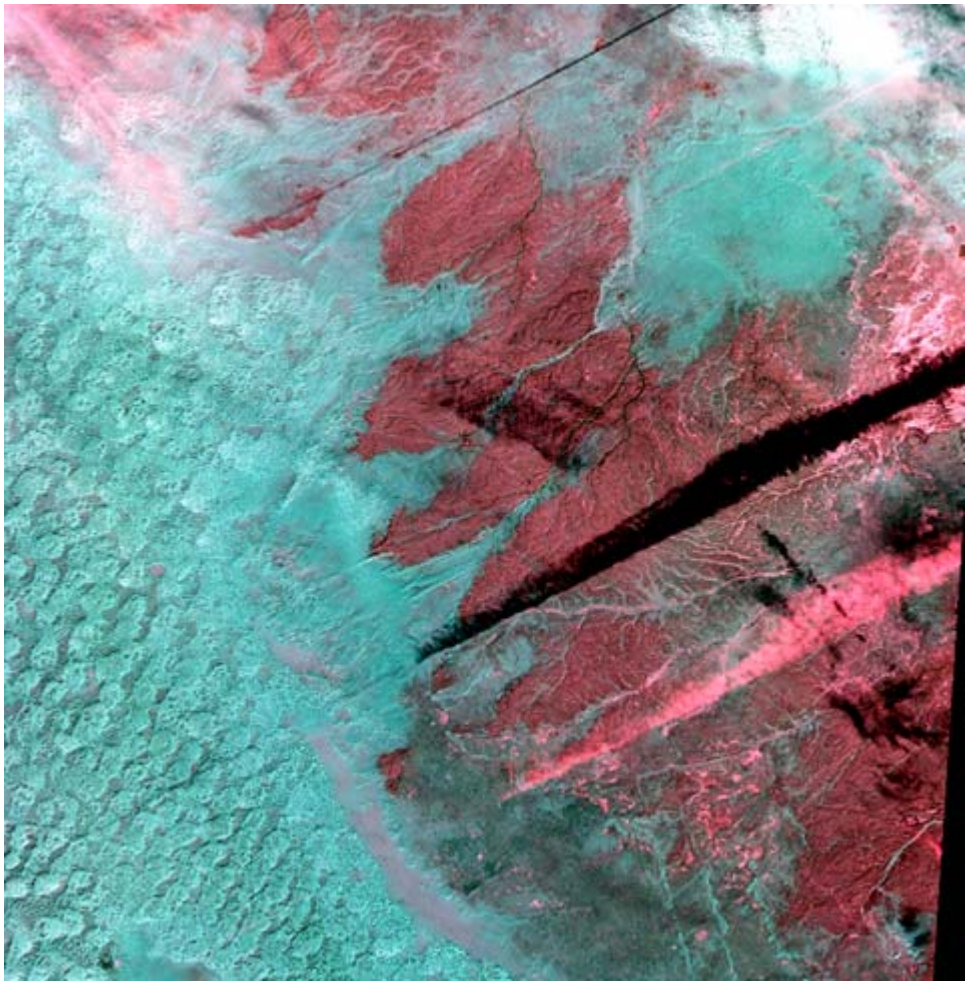

Figure 16. ASTER image from Saudi Arabia on 15 November 2001 showing contrails. Smaller contrail in upper portion of image was not sampled due to possible contamination due to cirrus clouds

2. Ground Truth

The Solar Village AERONET site in central Saudi Arabia was used for verification. All samples taken were located within 200 kilometers of the AERONET site. The ASTER imagery was collected at 07:50 UTC and AERONET measurements from 07:34 UTC were used for verification. Table 22 depicts the derived AERONET values that were derived and used for verification.

Table 22. AERONET integrated AOD for 15 November 2001 over Saudi Arabia.

Channel	Green	Red	NIR
Band(microns)	0.520-0.600	0.630-0.690	0.760-0.860
AOD	0.3895	0.3849	0.3796

3. Results

Table 23 shows the average AOD and standard deviation from 15 November 2001. The results correlated well to AERONET measurements as shown in Figure 17, with all three wavelengths measured between 0.03 and 0.04.

Table 23. Shadow Method AOD results from 15 November 2001 over Saudi Arabia.

Channel	Green	Red	NIR
Average	0.3272	0.3247	0.3526
Standard Deviation	0.0627	0.0694	0.0723

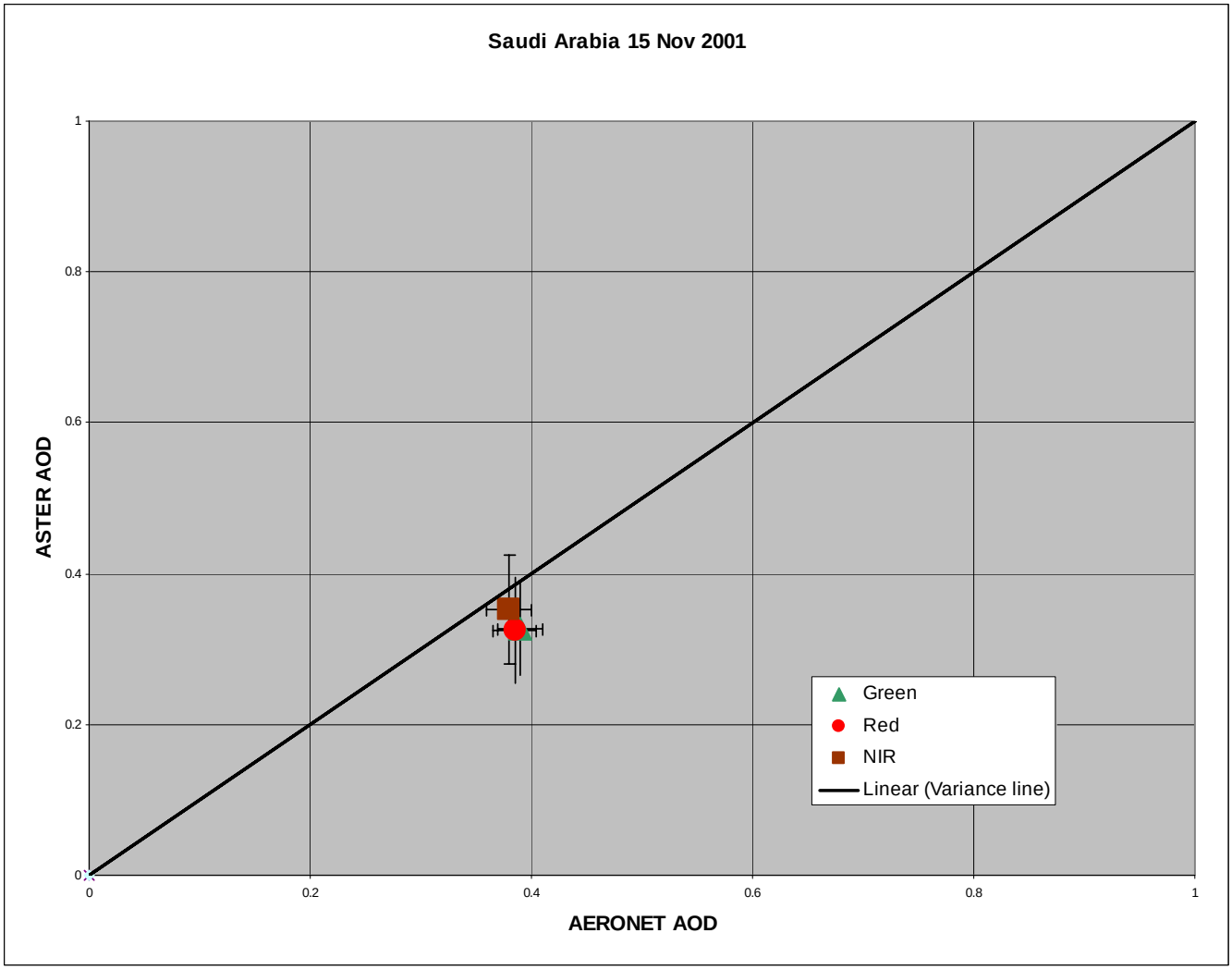

Figure 17. Comparison of ASTER AOD measurements to AERONET derived AOD measurements over Saudi Arabia on 15 November 2001. The standard error of the samples is annotated as a vertical error bar. The uncertainty of the AERONET measurement, ±0.2, is annotated as a horizontal error bar.

4. Summary

All three channels provided very similar results including a low bias as seen in imagery from other sensors. This case was the first to sample cloud shadows other than that from cumulus clouds. It appears that the results using this method are independent of cloud type, which was hypothesized as described in Part II.

C. MODIS

MODIS imagery introduces new challenges compared to other imagery. At 250 meter and 500 meter resolution, the sample quality is relatively poor (as depicted in Figure 18), because at times, cloud shadows were sub-pixel, meaning the radiance inside and outside the shadow was averaged and could not be used with confidence. Great care was taken to ensure there was no contamination of direct radiation into the shadow of any samples. Therefore, samples were biased towards the center of the shadow and may have resulted in slightly low optical depth measurements. Also, since MODIS imagery has a wider field of view, samples had to be taken farther away from the AERONET sites that were considered to be representative. All of these analysis constraints could result in the data being slightly skewed.

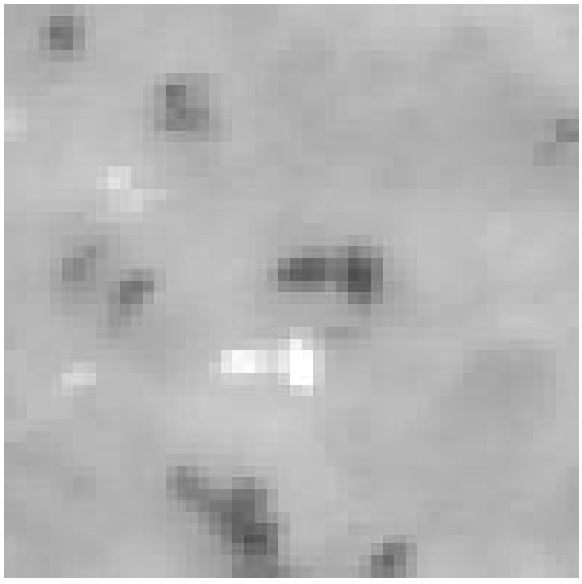

Figure 18. MODIS imagery at 250-meter resolution showing blurring of shadows.

1. United Arab Emirates, 28 November 2007

a. Overview

A series of cloud streets (Figure 19) over UAE on this day provided shadows large enough for sampling. MODIS data sampled consisted of three visible and two near-infrared channels. Ten samples were collected and analyzed over UAE.

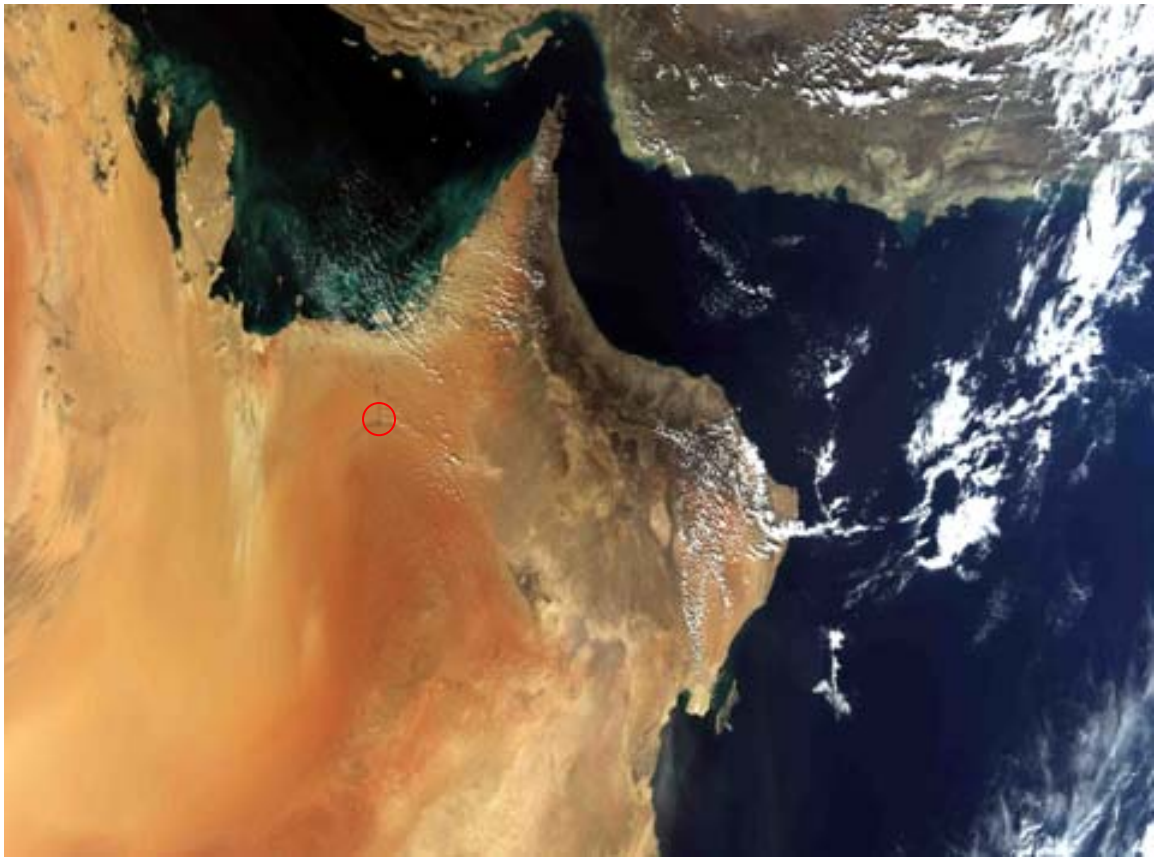

Figure 19. MODIS overview of southeastern Saudi Arabia and United Arab Emirates for 28 November 2007. Red circle denotes location of Mezaira AERONET site.

b. Ground Truth

The Mezaira AERONET site in UAE was used for verification. All samples taken were located within 115km of the AERONET site. The MODIS imagery

was collected at 09:40 UTC and AERONET measurements from 09:44 UTC were used for verification. The table below depicts the derived AERONET values that were derived and used for verification.

Table 24. AERONET integrated AOD for 28 November 2007 over UAE.

Channel	Blue	Green	Red	NIR	SWIR
Band(microns)	0.459-0.479	0.545-0.565	0.620-0.670	0.841-0.876	1.628-1.652
AOD	0.2693	0.2453	0.2254	0.1927	0.1535

c. Results

Table 25 shows the average AOD and standard deviation results from 28 November 2007. Table 26 displays the values of all samples taken along with distance from the AERONET site. Figure 20 illustrates the final results as compared to AERONET measurements. All samples were taken within 115 km of the AERONET site. This resulted in a relatively high standard deviation across all channels. However, the final results are within approximately 30% of AERONET readings and are considered to be an acceptable tolerance.

Table 25. Shadow Method AOD results from 28 November 2007 over UAE.

Channel	Blue	Green	Red	NIR	SWIR
Average	0.2590	0.1831	0.1538	0.1464	0.2427
Standard Deviation	0.0853	0.0654	0.0592	0.0557	0.0622

Table 26. Table showing sample values and distance from AERONET site used for representativeness on 28 November 2007.

Distance (km)	Blue	Green	Red	NIR	SWIR
30	0.187237	0.127918	0.10329	0.102298	0.137358
12	0.300662	0.192036	0.150376	0.13524	0.256455
23	0.188798	0.137379	0.092908	0.091574	0.183849
32	0.267338	0.188262	0.182075	0.174045	0.295472

72	0.381097	0.285869	0.212853	0.198789	0.256583
89	0.324361	0.201736	0.189455	0.182165	0.181745
113	0.229036	0.149146	0.121904	0.116721	0.153812
102	0.191062	0.132493	0.120002	0.115959	0.306717
77	0.236456	0.184951	0.223493	0.21183	0.359255
13	0.283965	0.230797	0.14149	0.135511	0.296426

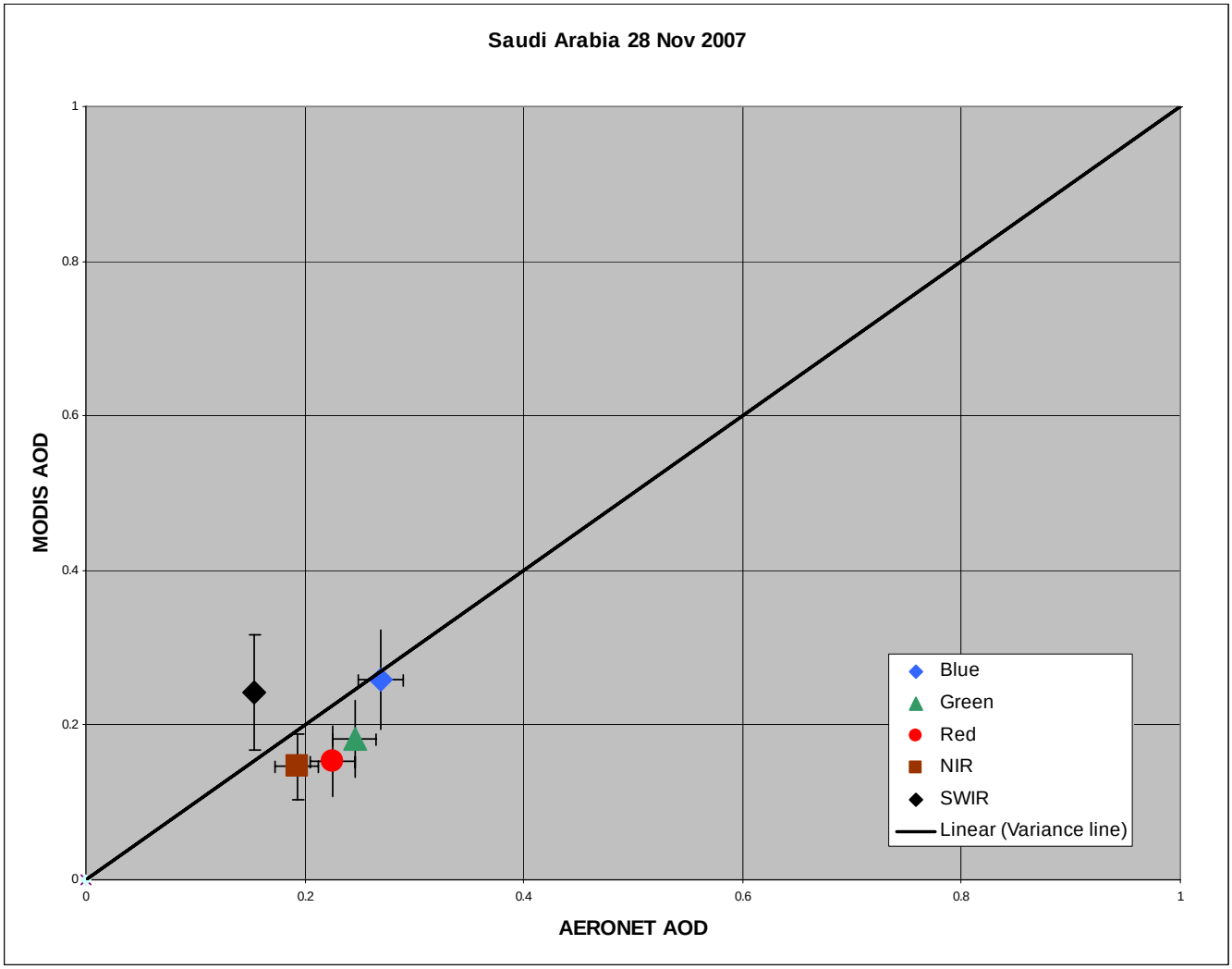

Figure 20. Comparison of MODIS AOD measurements to AERONET derived AOD measurements over UAE on 28 November 2007. The standard error of the samples is annotated as a vertical error bar. The uncertainty of the AERONET measurement, ±0.2, is annotated as a horizontal error bar.

d. Summary

This was the first time the SWIR channel (1628 nm) was sampled and compared to AERONET, and it provided results much different than the visible and NIR channels. With the exception of the SWIR, there were low biases as compared to AERONET. As with QuickBird, the bias decreased with decreasing wavelength. The SWIR channel had a high bias. This could be due to how sensitive the SWIR band is to single-scatter albedo. A sensitivity analysis was performed to see how each channel responded to the single-scatter albedo (SSA) value used in the calculation of optical depth. Values between 0.70 and 0.95 were input and the same sample shaded and unshaded regions were tested. Results showed that between SSA's of 0.70 and 0.95, the SWIR band only decreased by two percent of its AOD value, compared to nearly 13 percent for the blue channel. Figure 21 details all channels and their response to SSA. For this case study, an SSA of 0.97 was used. As a comparison, if an SSA of 0.88 was used in this case, all channels would be slightly higher in value. However, the SWIR channel would more closely match the response of the other channels.

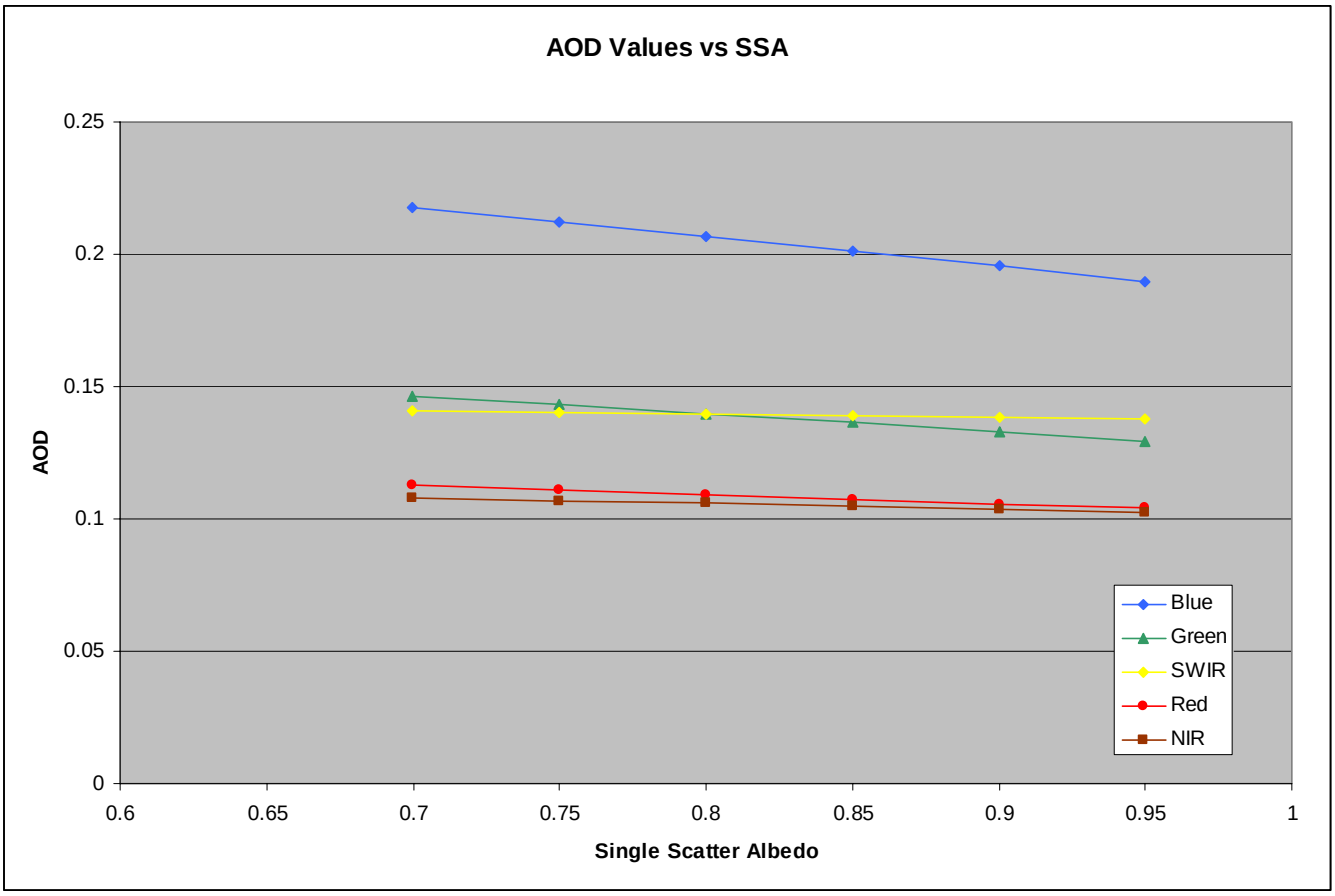

Figure 21. Sensitivity analysis of each channel as single scatter albedo changes. Shorter wavelengths are more sensitive to changes in albedo than longer wavelengths.

2. United Arab Emirates, 07 January 2008

a. Overview

This date was chosen due to a dust storm moving through the region, resulting in extremely high optical depth readings from AERONET sites around the region. Visibility dropped as low as 500 meters in the region as the system passed. Eight samples were taken throughout UAE and compared to AERONET measurements. Figure 22 displays an overview of the region during this time. Heavy dust is clearly visible over UAE and the Persian Gulf.

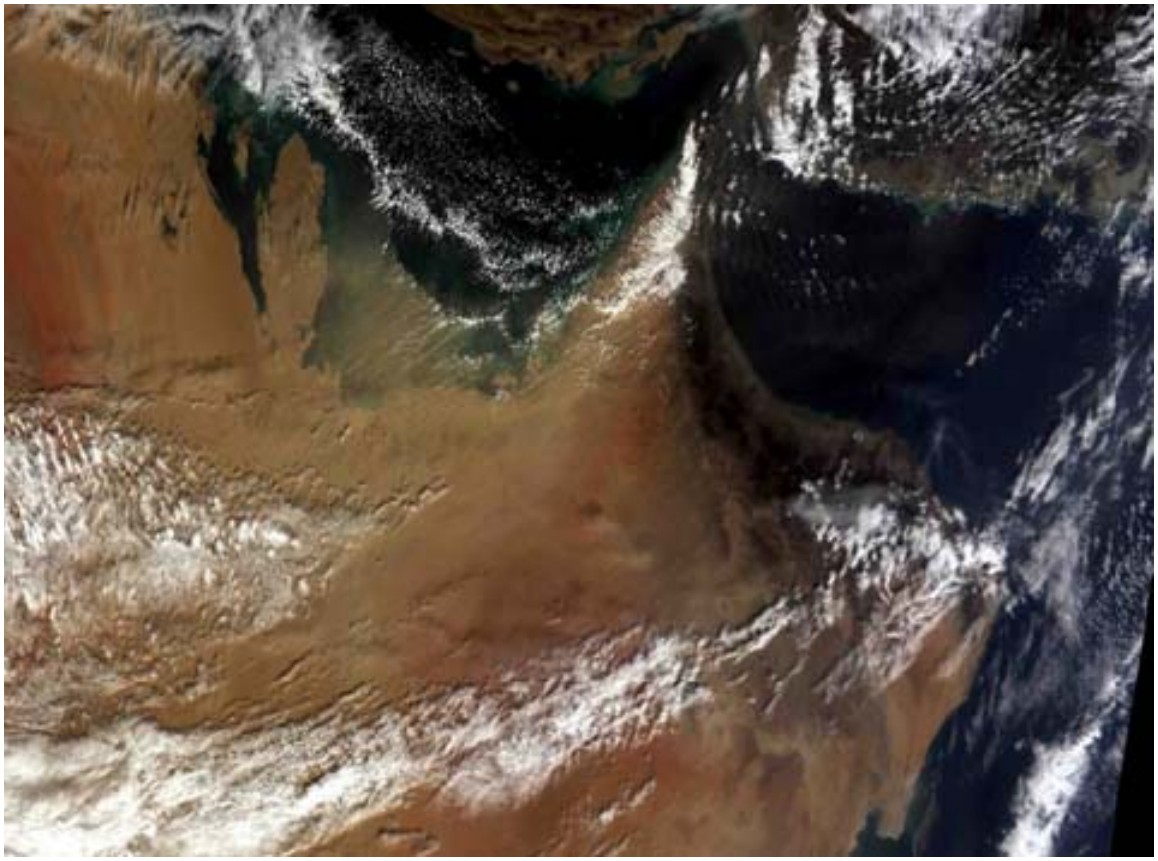

Figure 22. MODIS overview of southeastern Saudi Arabia and United Arab Emirates for 7 January 2008.

b. Ground Truth

As with the 28 November 2007 collection, the Mezaira AERONET site was used for verification. The MODIS imagery was collected at 07:20 UTC. AERONET measurements were available for 06:35 and 07:40 UTC. Looking at the trend of AERONET measurements in Figure 23, there is a fairly steady consistency in the increase in AOD values. Therefore, an interpolation of AOD to the time of the MODIS pass was calculated using the data below. Table 27 displays the AOD values used after interpolation.

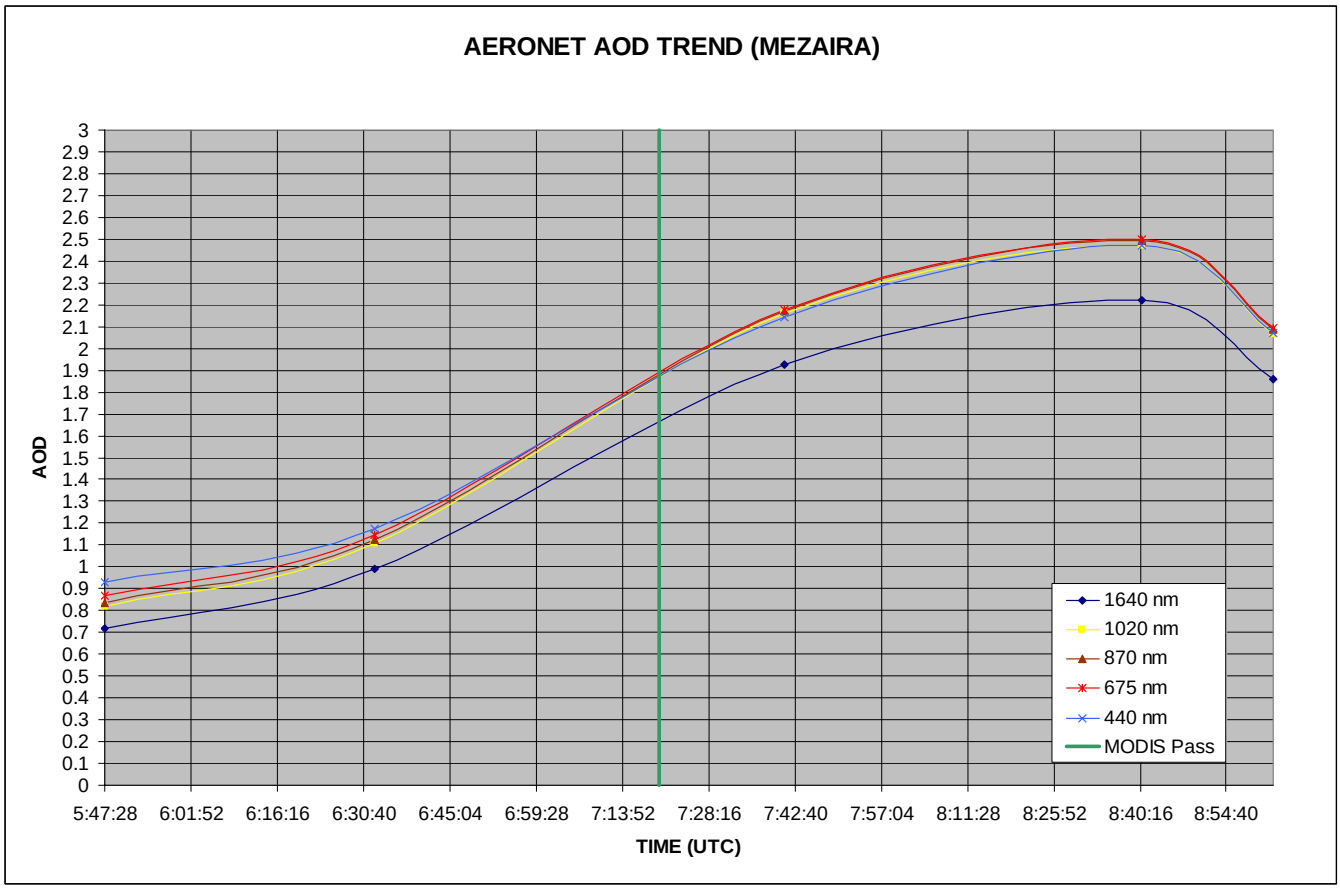

Figure 23. Aerosol optical depth trend for Mezaira AERONET site sorted by wavelength. The vertical line indicates the time of the MODIS pass which corresponds with the time of greatest optical depth change.

Table 27. AERONET integrated AOD for Mezaira AERONET site on 7 January 2008.

Channel	Blue	Green	Red	NIR	SWIR
Band(microns)	0.459-0.479	0.545-0.565	0.620-0.670	0.841-0.876	1.628-1.652
AOD	1.874	1.874	1.874	1.873	1.670

c. Results

Table 28 shows the average AOD and standard deviation results from 7 January 2008. Table 29 displays the values of all samples taken along with distance from

the AERONET site. Figure 24 displays the results from this case as compared to AERONET. Measurements across all wavelengths varied between approximately 0.025 and 0.07, with no correlation to AERONET readings or distance the sample was taken from the AERONET site.

Table 28. Shadow Method AOD results from 7 January 2008 over UAE.

Channel	Blue	Green	Red	NIR	SWIR
Average	0.3843	0.4756	0.2617	0.2486	0.6759
Standard Deviation	0.0671	0.0894	0.0645	0.0592	0.0941

Table 29. Table showing sample values and distance from AERONET site used for representativeness on 7 January 2008.

Distance (km)	Blue	Green	Red	NIR	SWIR
102	0.297319	0.302817	0.172958	0.167105	0.492955
92	0.44272	0.548927	0.360807	0.343986	0.752129
178	0.48792	0.594648	0.301089	0.281448	0.799207
214	0.313959	0.419795	0.19463	0.186429	0.617527
119	0.339373	0.445519	0.213703	0.205816	0.644441
165	0.372448	0.479097	0.301156	0.284481	0.679793
216	0.436157	0.523349	0.250541	0.24493	0.728935
237	0.384776	0.491032	0.299228	0.274799	0.691975

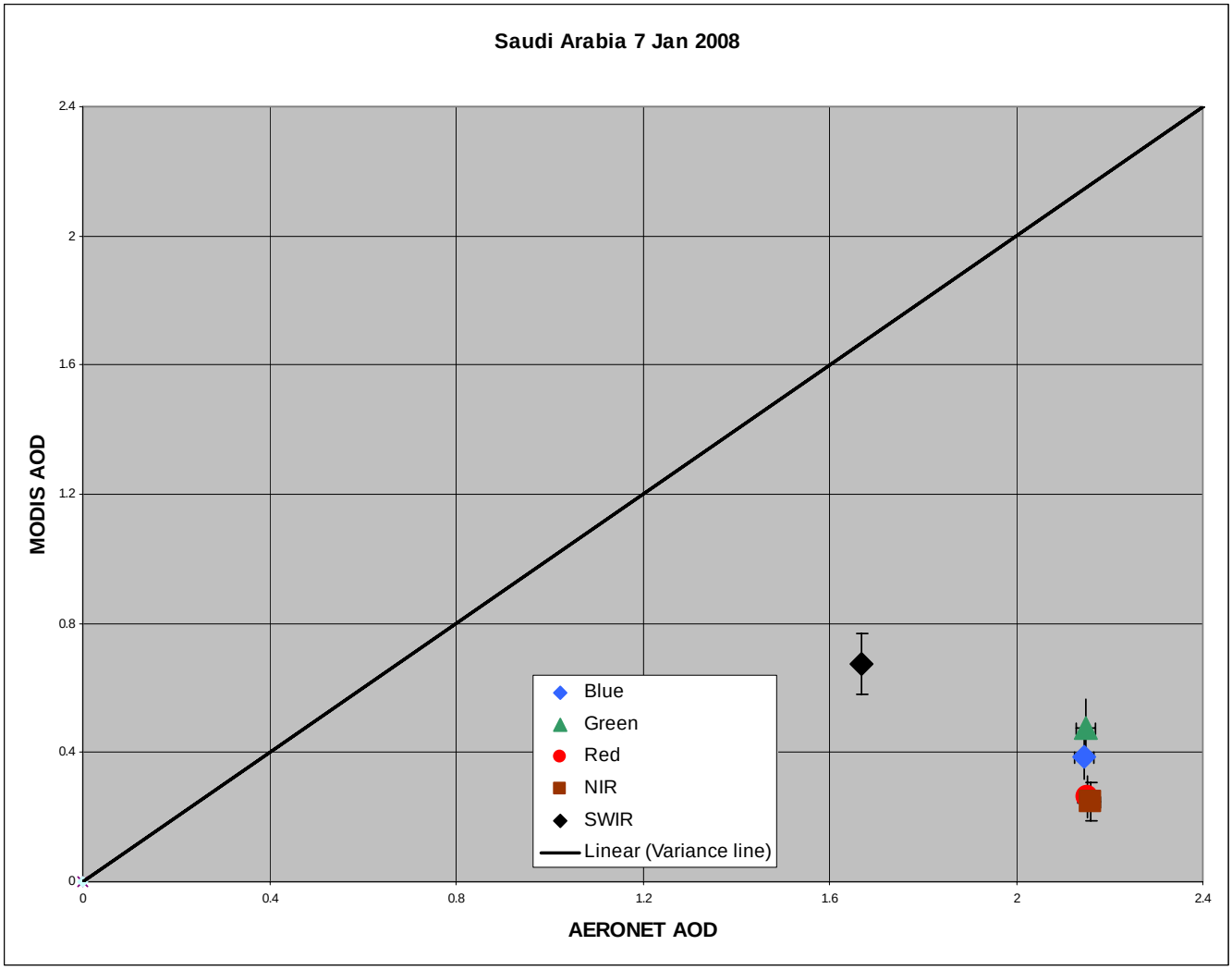

Figure 24. Comparison of MODIS AOD measurements to AERONET derived AOD measurements over UAE on 7 January 2008. The standard error of the samples is annotated as a vertical error bar. The uncertainty of the AERONET measurement, ±0.2, is annotated as a horizontal error bar.

d. Summary

This case provided the highest AOD measurements of any using this method to date. Results had no consistency as in other cases and a reassessment was done. First, soundings from the region were analyzed. Figure 25 displays a sounding from King Fahd International Airport, Saudi Arabia. An inversion is present at 860 meters (2820 feet). This can reasonably be considered to be the height of the top of the

dust layer. Cloud top temperatures and corresponding heights in the region were determined using Channel 31 from MODIS. The analysis showed cloud top temperatures between zero and -3 C, corresponding to cloud top heights between 6500 and 9800 feet. This was verified by measuring the distance between the sample cloud tops and corresponding shadows in ENVI. Since the solar angle is known, the distance from the cloud top directly to the ground can be calculated. Observations from the region showed cloud bases between 4000 and 5000 feet as shown in the surface observations from Abu Dhabi in Table 30. For example, the observation from 09:00 UTC (highlighted) depicts scattered clouds at 4800 feet and visibility restricted to 2000 meters due to dust. The clouds in this observation are above the height of the top of the dust layer.

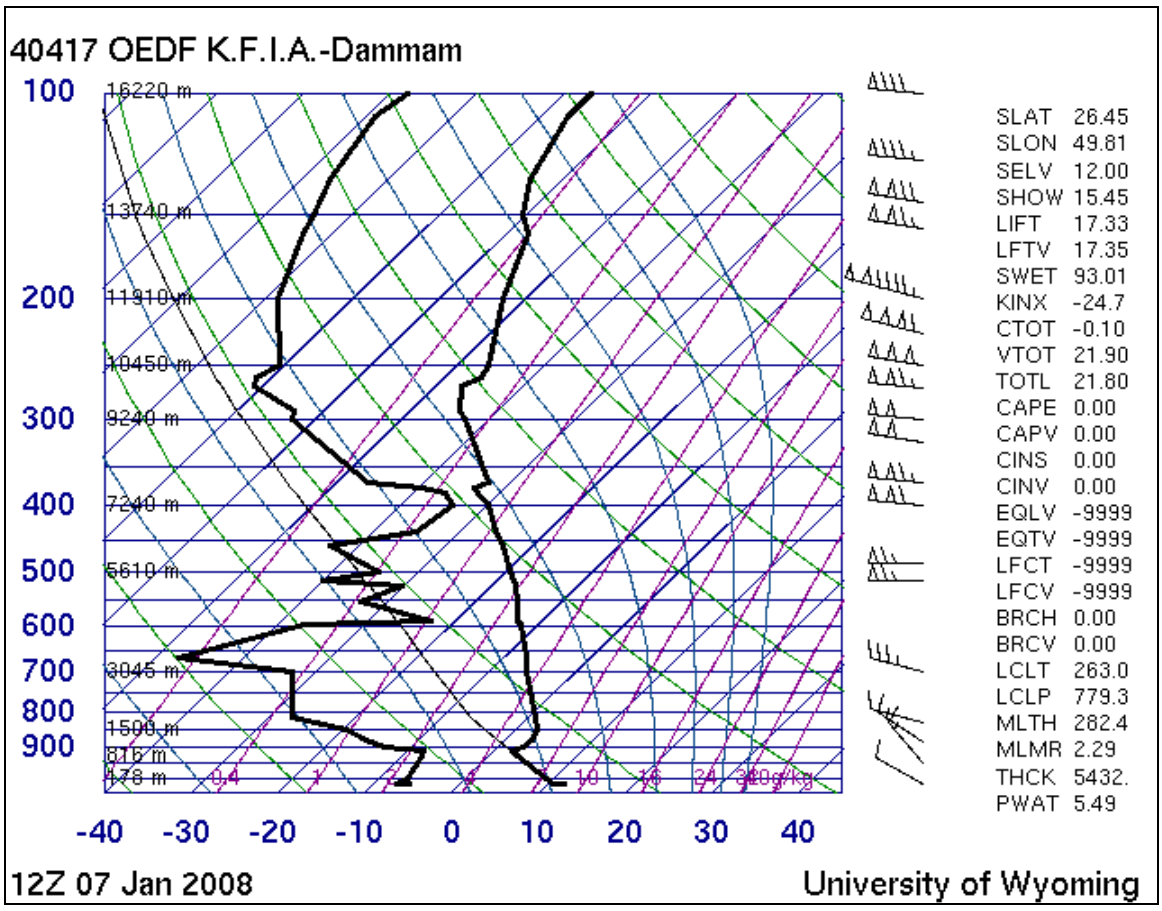

Figure 25. Upper-air sounding from King Fahd International Airport, Saudi Arabia, showing presence of inversion in lower atmosphere. This can be considered to be approximately the height of the top of the dust layer.

Table 30. Surface Observations for Abu Dhabi, UAE, between 00:00 UTC and 13:00 UTC on 7 January 2008.

Observations for ABU, United Arab Emirates (OMAA)
OMAA 071300Z 33012KT 9999 FEW040 SCT043 17/08 Q1017 A3003 NOSIG
OMAA 071200Z 33013KT 9999 FEW043 SCT046 18/07 Q1016 A3002 NOSIG
OMAA 071100Z 31015KT 7000 SCT043 18/06 Q1016 A3002 NOSIG
OMAA 071000Z 32015KT 5000 DU SCT048 19/05 Q1016 A3003 BECMG 7000
OMAA 070915Z 31015KT 3000 DU SCT048 18/04 Q1017 A3003 BECMG 5000
OMAA 070900Z 31013KT 2000 DU SCT048 18/07 Q1017 A3004 BECMG 3500
OMAA 070800Z 31015KT 1600 R13/1800U R31/1400U DU SKC 18/02 Q1018 A3007 BECMG 3500
OMAA 070700Z 30016KT 1400 R13/1200D R31/1100D DU VV009 18/06 Q1019 A3009 NOSIG
OMAA 070635Z 29017KT 1400 R13/1400D R31/1500D DU VV009 18/06 Q1018 A3009 NOSIG
OMAA 070600Z 29017KT 2800 DU SCT045 17/07 Q1018 A3008 TEMPO 1500
OMAA 070521Z 29017KT 2900 DU SCT045 17/06 Q1018 A3008 BECMG 1800
OMAA 070500Z 29015KT 4500 DU SCT045 17/05 Q1018 A3007 NOSIG
OMAA 070400Z 30016KT 5000 DU FEW040 16/05 Q1017 A3006 NOSIG
OMAA 070300Z 30015KT 5000 DU FEW040 16/06 Q1017 A3003 TEMPO 4000
OMAA 070200Z 29019KT 6000 FEW040 16/07 Q1016 A3001 TEMPO 4000
OMAA 070100Z 28016KT 6000 FEW043 16/05 Q1016 A3000 TEMPO 4000
OMAA 070000Z 28016G27KT 4000 DU FEW043 17/07 Q1015 A2998 TEMPO 3000

Clouds over the Persian Gulf were also studied to determine where the clouds were in relation to the dust layer. The MODIS NIR channel from a clear day over the region was studied to determine a baseline for how dark the Persian Gulf appears in this channel and how much turbidity is present under normal conditions. It was determined the water is dark and there is no turbidity under normal conditions. Therefore, any color change in this channel occurring over water on 7 January 2008 was strictly due to dust effects. By studying the cloud field further, there appears to be shadowing cast upon the dust layer over the water as shown in Figure 26.

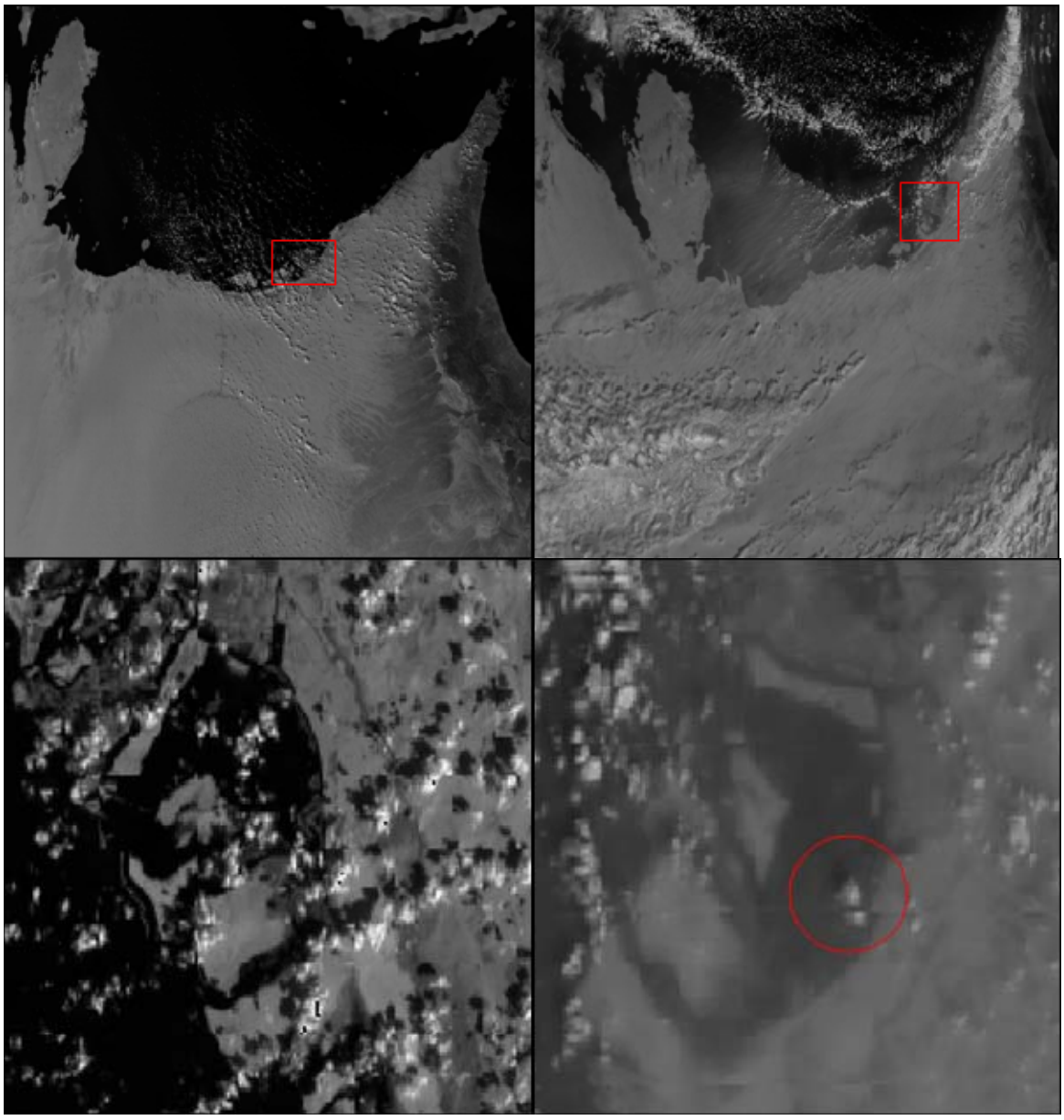

Figure 26. MODIS NIR imagery over UAE illustrating dust effects. Red boxes denote zoomed in areas. The image at top left shows the clarity and darkness of the Persian Gulf under normal conditions. The image at top right clearly displays the dust over the water on 7 January 2008. At bottom left, note how clouds do not cast shadows over water under clear conditions. At bottom right, cloud over same location on 7 January 2008 casting shadow onto dust layer.

After this analysis, it appears the clouds were just above the dust layer. Results were not consistent with the AERONET site measurements because the cloud

shadow was not being cast onto the ground but rather onto the layer of dust. Therefore, the radiance values extracted from the imagery are not from within the heavy aerosol region but from the relatively dust-free layer just above it, resulting in lower optical depth values than the AERONET sun photometer which is measuring from the surface and within the dust layer.

3. Solar Village, Saudi Arabia, 31 August 2007

a. Overview

The final MODIS image sampled was over the interior of Saudi Arabia on 31 August 2007. Nine samples of shadows were taken near Solar Village on this day. Figure 27 depicts an overview of the region for this day.

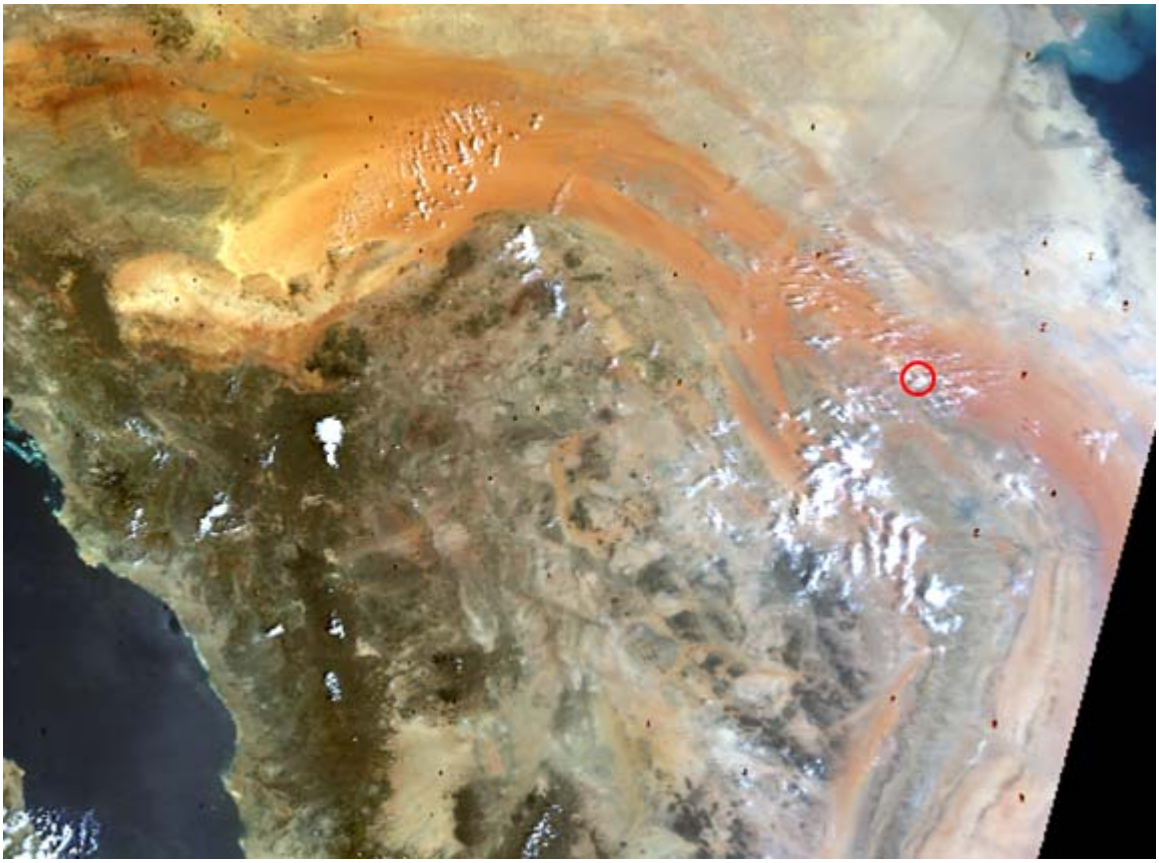

Figure 27. MODIS overview of southeastern Saudi Arabia and United Arab Emirates for 31 August 2007. Red circle denotes location of Solar Village.

b. Ground Truth

The MODIS pass was at 08:15 UTC and AERONET measurements from 08:11 UTC at Solar Village were used for verification. The table below depicts the derived AERONET values that were derived and used for verification.

Table 31. AERONET integrated AOD for 31 August 2007 over Saudi Arabia.

Channel	Blue	Green	Red	NIR	SWIR
Band(microns)	0.459-0.479	0.545-0.565	0.620-0.670	0.841-0.876	1.628-1.652
AOD	0.5793	0.4949	0.4293	0.3297	0.2161

c. Results

Table 32 shows the average AOD and standard deviation from 31 August 2007. Table 33 displays the values of all samples taken along with distance from the AERONET site. All samples from MODIS were taken within 230 km of Solar Village. Looking at Figure 28, the results show a consistent linear pattern across all channels. All measurements in the solar channels differed from AERONET measurements by approximately 0.10.

Table 32. Shadow Method AOD results for 31 August 2007 over Saudi Arabia.

Channel	Blue	Green	Red	NIR	SWIR
Average	0.4806	0.3951	0.3351	0.2759	0.2472
Standard Deviation	0.0993	0.0804	0.0466	0.0367	0.0548

Table 33. Table showing sample values and distance from AERONET site used for representativeness on 31 August 2007.

Distance (km)	Blue	Green	Red	NIR	SWIR
149	0.412821	0.372875	0.313729	0.274091	0.284307
210	0.479343	0.379619	0.337976	0.260843	0.228028
196	0.599619	0.469277	0.314779	0.263182	0.225131
201	0.452865	0.364047	0.236566	0.203568	0.226254
174	0.503887	0.442844	0.34729	0.275898	0.304273
149	0.625045	0.495607	0.410287	0.344153	0.314104
211	0.546262	0.464365	0.357971	0.290347	0.295248
125	0.331406	0.247622	0.341427	0.278375	0.157708
229	0.374231	0.320021	0.355737	0.293168	0.189958

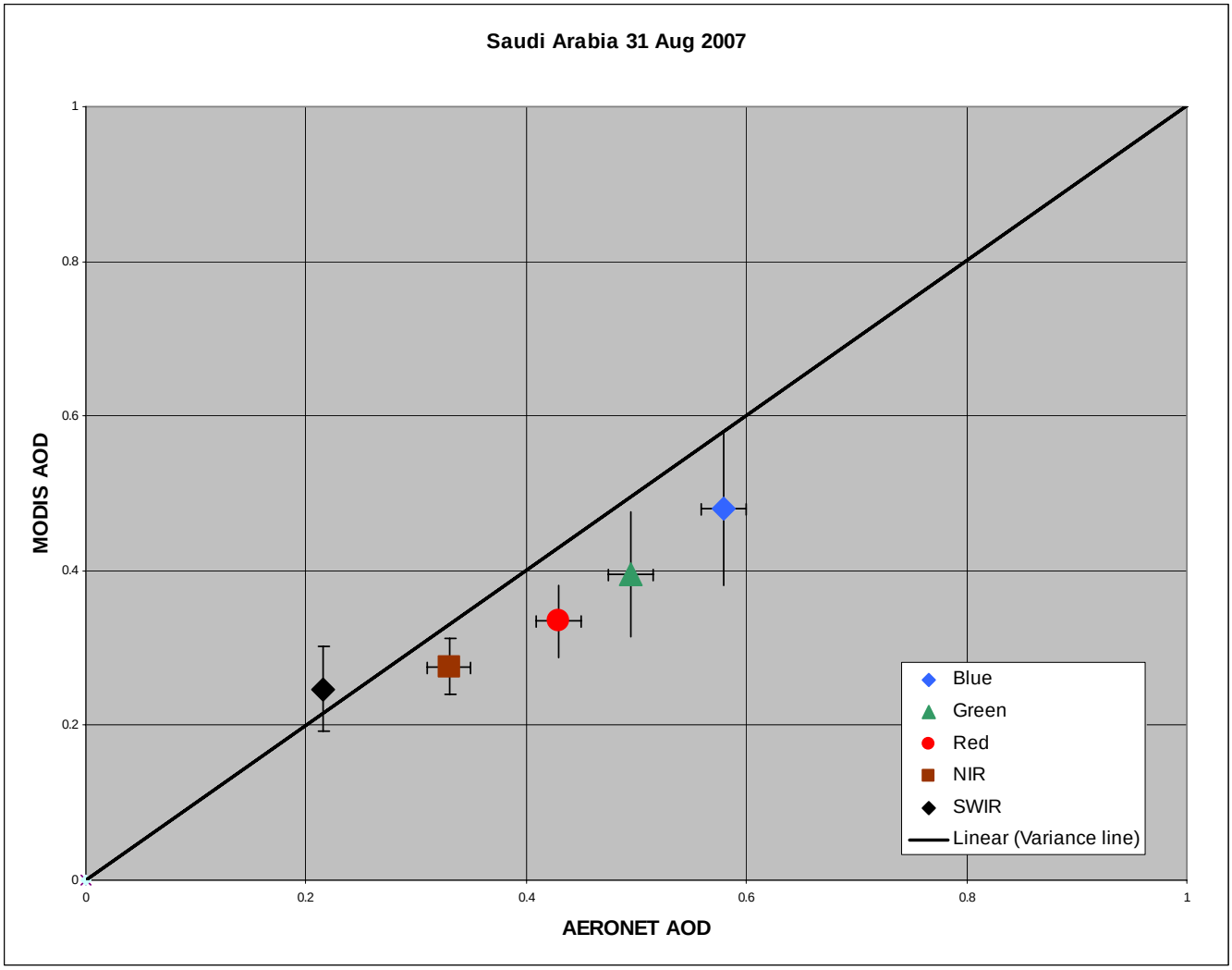

Figure 28. Comparison of MODIS AOD measurements to AERONET derived AOD measurements over Saudi Arabia on 31 August 2007. The standard error of the samples is annotated as a vertical error bar. The uncertainty of the AERONET measurement, ±0.2, is annotated as a horizontal error bar.

d. Summary

As in the 28 November 2007 MODIS case study, all channels had a slight low bias with the exception of SWIR, which had a high bias. Again, this bias in the SWIR can possibly be attributed to the decreased sensitivity to SSA.

D. IKONOS—31 AUGUST 2007

1. Overview

The IKONOS imagery was collected over the Saudi Arabian desert on 31 August 2007. Nine samples of cloud shadows were collected and analyzed. After analyzing MODIS imagery and surface observations, it was decided although the samples taken were approximately 450 km away from Solar Village, they can be considered fairly representative of conditions at the AERONET site.

2. Ground Truth

The IKONOS pass was at 07:22 UTC and AERONET measurements from Solar Village at 07:25 UTC were used for verification. The table below depicts the derived AERONET values that were derived and used for verification.

Table 34. AERONET integrated AOD for 31 August 2007 over Saudi Arabia.

Channel	Blue	Green	Red	NIR	Panchromatic
Band(microns)	0.445-0.516	0.506-0.595	0.632-0.698	0.757-0.853	0.527-0.929
AOD	0.5217	0.4669	0.4100	0.3422	0.3790

3. Results

Table 35 shows the average AOD and standard deviation from 31 August 2007. The results correlated extremely well to AERONET measurements as shown in Figure 29, differing by a maximum of 0.04 and showing a fairly consistent pattern as wavelength increases.

Table 35. Shadow Method AOD results for 31 August 2007 over Saudi Arabia.

Channel	Blue	Green	Red	NIR	Panchromatic
Average	0.5103	0.4259	0.3777	0.3390	0.3596
Standard Deviation	0.0545	0.0504	0.0487	0.0455	0.0500

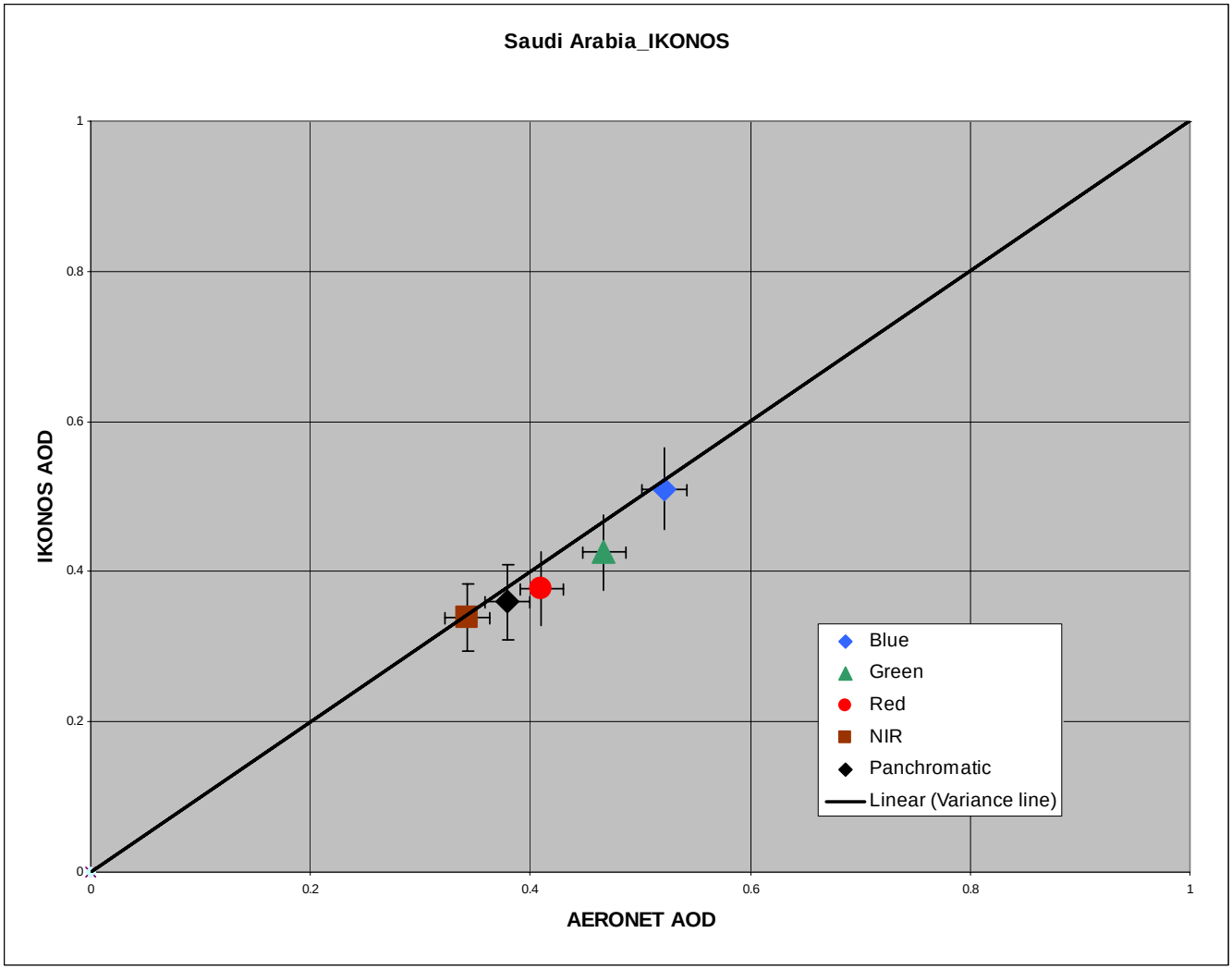

Figure 29. Comparison of IKONOS AOD measurements to AERONET derived AOD measurements over Saudi Arabia on 31 August 2007. The standard error of the samples is annotated as a vertical error bar. The uncertainty of the AERONET measurement, ±0.2, is annotated as a horizontal error bar.

4. Summary

Out of all cases, these results most closely lined up with AERONET readings. There was very slight low bias in all channels. This correlation is most likely due to the high sensor resolution and confidence in samples taken as shadows were clear and there was no risk of contamination inside and outside the shadow.

THIS PAGE INTENTIONALLY LEFT BLANK

V. CONCLUSION

A. CONCLUSIONS

This is the third study of the Shadow Method and its performance under a variety of conditions. Vincent (2006) proposed the technique, performing sensitivity analyses and initial case studies using QuickBird imagery. Evans (2007) followed by studying how the technique performs in an urban environment with multiple surface types. This thesis shifts the focus from shadows generated by ground-based objects using QuickBird imagery and expands it to cloud-generated shadows using additional data sources. This means extremely high-resolution satellite imagery is not necessarily required since clouds can generate much larger shadows than buildings. Therefore, three additional sensors were analyzed: ASTER, MODIS, and IKONOS. The results in this thesis are varied due to using multiple sensors and the varying environmental conditions that were occurring. Ultimately, the Shadow Method appears to have promise when applied to cloud shadows. It also appears that it can be used with sensors of varying spatial resolutions with some degree of confidence. Imagery resolutions sampled varied between 0.6 meter and 500 meter resolution and with the exception of the heavy dust case, results fell within reasonable standards. From a sampling standpoint, 500-meter resolution appears to be the absolute upper limit where samples could be considered accurate.

This technique was tested on five different days using four different sensors. AERONET measurements ranged from 0.15 to nearly 1.9 over all cases. Again, with the exception of the heavy dust case, all results compared well. The heavy dust case was particularly important because it highlighted Vincent's analysis of the limitations of the Shadow Method. Vincent (2006) determined that

> The upper limit of this method is determined by maximizing the cosine of solar and sensor zenith angles, maximizing surface reflectance, and minimizing mean aerosol reflectance. Based on such parameters, the upper limit of the shadow-based AOD retrieval method is approximately 2.0. At this AOD, the surface is effectively obscured and shadows are not distinguishable.

While Vincent's calculations are correct and this technique is limited to the ability to discern between shadow and surface, there is a second part to the limitations of this method. The Shadow Method also has an upper limit which is based on the location of the cloud relative to an aerosol layer. If there is a well-defined aerosol layer and the cloud generating the shadow is located entirely above this layer, AOD measurements can be skewed. In the heavy dust case, the surface was not a factor in the samples taken due to the thick layer of dust over the region. This dust layer essentially served as a secondary "surface" for cloud shadows to be cast upon.

Across all sensors, there was a low bias across nearly all channels similar to what Evans (2007) observed. The SWIR channel was slightly higher in the MODIS cases. Vincent (2006) and Evans (2007) offered three reasons for the low bias. The first is an unrepresentative aerosol model and determining the correct inputs for single scatter albedo and asymmetry parameters. This will have some effect on the results, but overall it is a small factor in the final output. The second possibility for low bias was attributed to buildings blocking the sky and affecting scattering in the sample area. This may contribute to lower results when in an urban environment. The third possibility was assuming a lambertian reflectance when specular reflectance of the surface may be more representative. This is more important when using QuickBird and IKONOS imagery, where individual surfaces are able to be distinguished.

B. FUTURE RESEARCH

While the final results are comparable to AERONET, studies need to be done on how to minimize the low bias consistently seen in QuickBird imagery. This should be conducted in a controlled environment where elements such as type of reflection can be better controlled. Optical depth measurements should be taken at the test site where shadows are being generated.

Focus should also be directed towards automation of this detailed process. As Vincent (2006) explained, this method will have greater usefulness if sampling can be automated. Currently, by the time imagery is received, samples are taken, and AOD is calculated, six to eight hours will have passed beyond the valid time of the imagery.

With quickly changing environmental conditions, the data would not provide much usefulness at that point except in post analysis of the event. Automation is a giant undertaking as it involves determining thresholds between radiance values to determine where shadows are if dynamic targeting is done. In the case of fixed targeting, suitable target shadows would need to be identified across multiple regions and "climatology" would need to be developed on the performance of these shadows. In both scenarios, studies need to be undertaken to determine if a correlation can be made between AOD and visibility.

One final area of study is the usefulness of future satellite imagery. High-resolution commercial satellite imagery is becoming more available as new satellites are launched. In September 2007, DigitalGlobe launched WorldView-1. This satellite provides panchromatic images only and currently features the highest resolution commercially available with a resolution of 0.5 meters. In 2008, DigitalGlobe will launch WorldView-2. This satellite will provide multi-spectral and panchromatic imagery in 1.84 meter and 0.46 meter resolutions, respectively (DigitalGlobe 2008). Also in 2008, GEOEYE will launch GeoEye-1 to complement IKONOS. This satellite will collect imagery in both multi-spectral and panchromatic bands at 1.65 meter and 0.41 meter resolutions, respectively (GEOEYE 2008). Once these two new satellites are launched, smaller shadow generators will be able to be sampled as shadows will be provided in resolutions never before seen. The Shadow Method should be tested with these new satellites to determine any limitations.

THIS PAGE INTENTIONALLY LEFT BLANK

LIST OF REFERENCES

Cotton, W.R., and R.A. Pielke, 1995: Human Impacts on Weather and Climate. Cambridge University Press, 296 pp.

de Leeuw, G., and R. Schoemaker, 2005: Retrieval of Aerosol Properties over Land and Water using (A)ATSR. Preprints. *MERIS- (A)ATSR Workshop*. Frascati, Italy, European Space Agency, 1-6.

DigitalGlobe, cited February 2008: QuickBird Imagery Products, Product Guide. [Available online at http://www.digitalglobe.com.]

DigitalGlobe, cited February 2008: WorldView-1 Products Quick Imagery Guide. [Available online at http://www.digitalglobe.com.]

Dombrock, R., 2007: Automating Shadow Method for AOD Retrieval. M.S. thesis, Department of Meteorology, Naval Postgraduate School, CA, 59 pp.

Fraser, R. S., Y. J. Kaufman, and R. L. Mahoney, 1984: Satellite measurements of aerosol mass and transport. *Atmos. Environ.*, **18**, 2577-2584.

Frolich, C., and G.E. Shaw, 1980: New determination of Rayleigh scattering in the terrestrial atmosphere. *Appl. Opt.*, **19**, 1773-1775.

Geoeye, cited February 2008: Geoeye Imagery Products: Geoeye-1. [Available online at http://www.geoeye.com/products/imagery/geoeye1/default.htm.]

Geoeye, cited February 2008: Geoeye Imagery Products: IKONOS. [Available online at http://www.geoeye.com/products/imagery/ikonos/default.htm.]

Goddard Space Flight Center (GSFC), cited 2008: Aerosol robotic network (AERONET). [Available online at http://aeronet.gsfc.nasa.gov/.]

Goddard Space Flight Center (GSFC), cited 2008: MODIS Web. [Available online at http://modis.gsfc.nasa.gov.] February 2008.

Hardin, M., and R. Kahn, cited 2008: What are Aerosols? Fact Sheet. NASA Earth Observatory. [Available online at http://earthobservatory.nasa.gov/Library/Aerosols/aerosol.html.]

Hsu, N. C., S. C. Tsay, M. D. King, and J. R. Herman, 2004: Aerosol properties over bright-reflecting source regions. *IEEE Trans. Geosci. Remote Sensing*, **42**, 557-569

ITT, cited February 2008: [Available online at http://www.ittvis.com/envi.]

Jet Propulsion Laboratory (JPL), cited 2008: Advanced Spaceborne Thermal Emission and Reflection Radiometer (ASTER). [Available online at http://asterweb.jpl.nasa.gov.]

Jet Propulsion Laboratory (JPL), cited 2008: Multi-angle Imaging Spectro Radiometer (MISR). [Available online at http://www-misr.jpl.nasa.gov/mission/minst.html.]

Kaufman, Y. J., and J. H. Joseph, 1982: Determination of surface albedos and aerosol extinction characteristics from satellite imagery. *J. Geophys. Res.*, **87**, 1287-1299.

Kaufman, Y. J. and C. Sendra, 1988: Algorithm for automatic atmospheric corrections to visible and near-IR satellite imagery. *Int. J. Remote Sens.*, **9**, 1357-1381.

Kaufman, Y. J. and D. Tanre, 1996: Strategy for Direct and Indirect Methods for Correcting the Aerosol Effect on Remote Sensing: From AVHRR to EOS-MODIS. *Remote Sens Environ*, **55**, 65-79.

Kaufman, Y. J., D. Tanre, L. A. Remer, E. F. Vermote, A. Chu, and B. N. Holben, 1997: Operational remote sensing of tropospheric aerosol over land from EOS moderate resolution imaging spectroradiometer. *J. Geophys. Res.*, **102**, 17051-17067.

Martonchik, J. V., Diner, D. J., Kahn, R., and Gaitley ,B., 2004: Comparison of MISR and AERONET aerosol optical depths over desert sites. *J Geophys. Res.*, **31**, L16102, 1-4.

Reid, J. S., and Coauthors, 2004: Science Plan: United Arab Emirates Unified Aerosol Experiment. Naval Research Laboratory. [Available online at http://www.nrlmry.navy.mil/aerosol_web/Case_studies/uae2/UAE-SPlan-v1.0.pdf.] February 2008.

Russell, P. B., J. M. Livingston, E. G. Dutton, 1993: Pinatubo and pre-Pinatubo optical depth spectra: Mauna Loa measurements, comparisons, inferred particle size distributions, radiative effects, and relationship to lidar data. *J. Geophys. Res.*, **98**, 22969-22985.

Tanre, D., P. Y. Deschamps, C. Devaux, and M. Herman, 1988: Estimation of Saharan aerosol optical thickness from blurring effects in Thematic Mapper data. *J. Geophys. Res.*, **93**, 15955-15964.

The ATSR Project, cited 2008: Along Track Scanning Radiometer (ATSR). [Available on line at http://www.atsr.rl.ac.uk/]

Veefkind, J. P., deLeeuw, G., and Durkee, P.A., 1998: Retrieval of Aerosol Optical Depth over Land using two-angle view Satellite Radiometry during TARFOX, *Geophys Res. Lett.*, 25 3135-3138

Vincent, D. A., 2006: Aerosol optical depth retrievals from high-resolution commercial satellite imagery over areas of high surface reflectance. PhD Dissertation, Department of Meteorology, Naval Postgraduate School, CA, 5-10, 143-152.

Wehrli, C., 1985: Extraterrestrial Solar Spectrum – Publ. 615. Physical Meteorological Observatory and World Radiation Center, Davos Dorf, Switzerland.

THIS PAGE INTENTIONALLY LEFT BLANK

INITIAL DISTRIBUTION LIST

1. Defense Technical Information Center
   Ft. Belvoir, Virginia

2. Dudley Knox Library
   Naval Postgraduate School
   Monterey, California

3. Professor Philip A. Durkee (Code MR/DE)
   Department of Meteorology
   Naval Postgraduate School
   Monterey, California

4. Kurt Nielsen
   Department of Meteorology
   Naval Postgraduate School
   Monterey, California

5. Capt Perry C. Sweat
   Department of Meteorology
   Naval Postgraduate School
   Monterey, California